6 Atmospheric Aerosol Particles

Aerosol particles contribute to air pollution and negatively impact human health (e.g., Pöschl, 2005; Lelieveld et al., 2020). They also impact atmospheric chemistry and biogeochemical cycles (e.g., McNeill, 2017; Kanakidou et al., 2018; Zhang et al., 2022). Aerosols also play a key role in Earth's climate through aerosol-radiation and aerosol-cloud interactions (e.g., Lohmann and Feichter, 2005; Fuzzi et al., 2015). For example, to form a cloud droplet, an aerosol particle is required (Chapter 7). The process of cloud droplet formation on an aerosol particle occurs at the microscale but impacts macrophysical cloud properties, such as the horizontal and vertical extent, as well as the large-scale impacts of clouds on the energy budget.

In general, an aerosol is defined as a particle suspended in a carrier gas, in our case air. An aerosol particle can be solid, liquid, semi-solid, or glassy. Although the term *aerosol* includes both the particles and the carrier gas, in atmospheric science, it is common to use the term aerosol only for the condensed phase, that is, particles, and to neglect the carrier gas. Thus, a more precise definition would be to use the term *aerosol particles* to refer to any suspended particulate matter. Nonetheless, we use the terms, *aerosols*, *particles*, and *aerosol particles* interchangeably in this textbook. While cloud droplets and ice crystals generally occur in clearly defined entities (clouds and regions of precipitation), a background aerosol number concentration exists everywhere throughout the troposphere (Brock et al., 2021) and in the stratosphere.

Aerosol particles are typically described in terms of their chemical composition and physical properties, such as size, shape/morphology, and phase state (Section 6.1). Because aerosol particles vary in size from a few nanometers to several micrometers, it has been found useful to classify and describe them in terms of size ranges, so-called *aerosol modes*. These modes are useful when discussing aerosol particle number, surface, volume, and mass concentrations in using log-normal size distributions (Section 6.2).

Aerosol particles can be directly emitted into the atmosphere as particulate matter, termed *primary aerosols*, or formed in-situ within the atmosphere by oxidation of precursor gases followed by gas-to-particle conversion of the oxidation products, termed *secondary aerosols*. These formation mechanisms and the emissions of the most important aerosol types are the subject of Section 6.3. Aerosol particles are then removed from the atmosphere by dry and wet scavenging (Section 6.4). The difference between their formation and removal rates determines their abundance (*burden*) in the atmosphere as well as their atmospheric lifetime. In addition, the aerosol lifetime is strongly dependent not only on their size but also on their altitude in the atmosphere (Section 6.5). The chapter concludes with a summary of the most important aerosol processes in Section 6.6.

https://doi.org/10.1017/9781009485654.007 Published online by Cambridge University Press

6.1 Chemical and Physical Properties of Aerosol Particles

There exists a large variety of aerosol types in the atmosphere. These include sulfate (e.g., Ye et al., 2023), sea salt (e.g., Lewis and Schwartz, 2004), nitrate (e.g., Fowler et al., 2013), mineral dust (e.g., Mahowald et al., 2005; Choobari et al., 2014; Tang et al., 2016), biological (e.g., Fröhlich-Nowoisky et al., 2016), organic (e.g., Jimenez et al., 2009; Shrivastava et al., 2017), and black carbon particles (e.g., Bond et al., 2013). In addition, nano- and microplastic particles from anthropogenic emissions have also been identified in atmospheric aerosol particles (Trainic et al., 2020; Aeschlimann et al., 2022; Allen et al., 2022). Depending on the particle type, aerosols have different properties that determine their role in the atmosphere. For example, the optical properties determine their interactions with radiation and hence their climate impact (Section 12.1.1). Next, we discuss some of the fundamental chemical and physical properties that are often used to characterize aerosol particles and that govern their impacts.

6.1.1 Chemical Properties

Aerosol particles differ in their chemical composition. For example, a sulfuric acid particle nucleated from the oxidation products of its gaseous precursor sulfur dioxide (SO_2) can be described by a single chemical formula, namely H_2SO_4. By contrast, atmospheric organic aerosol (OA) is usually composed of a large range of organic compounds with different chemical formulae (Seinfeld and Pankow, 2003; Nozière et al., 2015; Ditto et al., 2018), even if they result from the oxidation of a single gaseous organic precursor compound. The wide range of compounds makes OA one of the most chemically complex aerosol types (Glasius and Goldstein, 2016). By contrast, the number of inorganic salts that are found in atmospheric aerosols is relatively small, with ammonium sulfate ($(NH_4)_2SO_4$), ammonium bisulfate (NH_4HSO_4), ammonium nitrate (NH_4NO_3), and sodium chloride (NaCl) being the major ones (Finlayson-Pitts and Pitts, 2000).

These different components can be present in the same or in different particles (Riemer et al., 2019). If different aerosol types get mixed in the same air mass, but with the individual particles consisting of just one specific species, the particle population is termed *externally mixed aerosol* (Figure 6.1a). On the other hand, an *internally mixed aerosol* contains different species within each individual particle (Figure 6.1b). In an aerosol population with internally mixed particles, the mixing ratio and species identities can vary from one particle to the next.

Figure 6.1d shows example microscopy images of externally and internally mixed particles (Fan et al., 2016). Internal mixing may be the result of atmospheric processes, such as the condensation of gaseous compounds onto the surface of a particle. Similarly, the evaporation of a cloud droplet that had collected different aerosol species can leave behind one particle combining the species previously present in the droplet.

In the atmosphere, the aerosol mixing state varies (e.g., Li et al., 2016; Liu et al., 2021), and aerosol populations often contain a mixture of particles that are internally and externally mixed, illustrated as the real-world mixture in Figure 6.1c.

Another important chemical property of aerosol particles is their acidity (or basicity), reflected in their pH value. Atmospheric aerosols generally tend to be acidic with pH mostly

https://doi.org/10.1017/9781009485654.007 Published online by Cambridge University Press

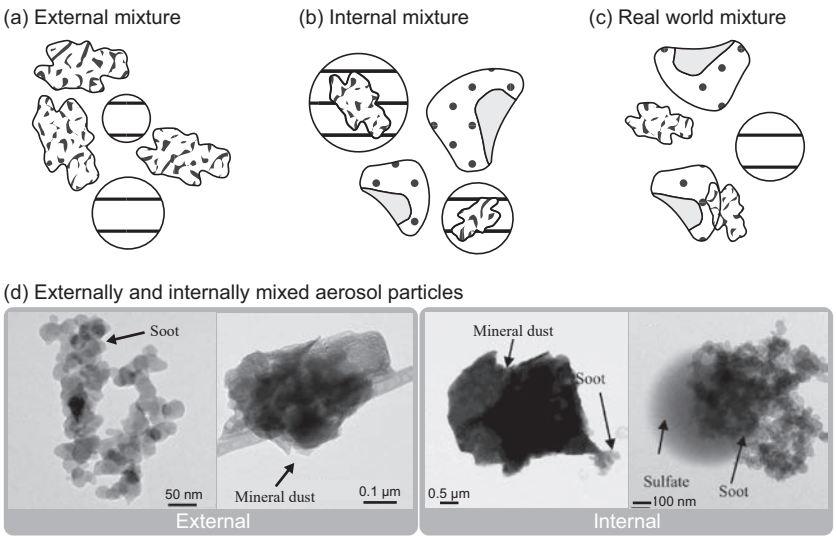


Figure 6.1 Illustration of an aerosol population that contains (a) externally mixed particles, (b) internally mixed particles, and (c) a mixture of internally and externally mixed particles. (d) Example of transmission electron microscopy images of externally and internally mixed particles. The aerosol components are labelled in the images and the scale bars denote approximate sizes for reference. Microscopy images are from Fabian Mahrt and Kouji Adachi (external mixtures) and taken from Fan et al. (2016) (internal mixtures).

below 8 (Pye et al., 2020). The aerosol pH depends on particle composition and size. Small aerosol particles that are dominated by sulfate, nitrate, and organics tend to be more acidic compared to larger particles that are dominated by dust and sea salt. Aerosol acidity also depends on the ambient temperature and RH: Aerosol acidity generally increases with increasing temperature and decreasing RH, leading to a seasonal cycle in aerosol pH with a minimum in summer (e.g., Guo et al., 2015). The effect of RH on aerosol acidity follows the water availability and aerosol liquid water content. The effect of temperature on aerosol acidity results from temperature affecting the thermodynamic equilibrium gas-particle partitioning, solubility and dissociation of key species, such as ammonia and nitric acid. Aerosol acidity impacts particle reactivity, mass, and composition, which in turn affect their ability to serve as CCN.

6.1.2 Physical Properties

The following physical characteristics are often used to characterize and describe atmospheric aerosols, depending on the process of interest: (i) size, surface area, and volume (or mass if the density is known), (ii) density, (iii) particle shape or morphology, which we use interchangeably, and (iv) phase state.

(i) Size is often considered the most important physical particle property, because a lot of other particle properties are closely related to it, such as aerosol lifetime in the atmosphere,

https://doi.org/10.1017/9781009485654.007 Published online by Cambridge University Press

their ability to act as CCN or INPs, as well as their optical (radiative) properties. However, the size of an aerosol particle is not unambiguously determined, but depends on the measurement method. Calculation of the particle size from the measured quantity usually requires an assumption on other particle properties, such as shape/morphology, density, and refractive index (Section 2.1.4). Therefore, standard values for these properties are often assumed in order to obtain an equivalent particle size for the specific measurement method (Baron and Willeke, 2001; Hinds and Zhu, 2022). The *equivalent radius* is the radius of a perfectly spherical particle that has the same value of a particular physical property (e.g., mass, density) as that of the irregularly-shaped (non-spherical) particle. An example of an equivalent size is the aerodynamic radius, r_{aero}. It is defined as the radius of a spherical particle with a density of $1000\,\mathrm{kg\,m^{-3}}$, that has the same settling velocity as the particle under consideration. Throughout this book, when using the term *size*, we refer to the spherical equivalent radius of the aerosol particle under consideration, if not stated otherwise.

Aerosol particles range in radii from a few nanometers to several tens of micrometers (Table 6.1). They are larger than typical atmospheric ions, which are usually below 0.5 nm in radius, and can be as large as cloud droplets ($r \sim 10\,\mu\mathrm{m}$).

Different emission sources produce aerosol particles of different sizes. Because of the size dependence of many atmospheric processes, various maxima and minima are typically found in size distributions of atmospheric aerosol particles. It has, therefore, been found useful to define certain aerosol modes on the basis of these size ranges, as listed in Table 6.1.

The lower boundary of the nucleation mode (a particle radius of 1.5 nm) has, on the one hand, been found to be a useful separator between large molecular clusters and small aerosol particles and, on the other hand, roughly corresponds to the experimental limit of traditional aerosol particle counters.

At the upper end of the aerosol size range, particles larger than 0.5 μm are categorized as coarse mode particles. Coarse mode particles are usually directly emitted into the atmosphere as primary aerosols. Particles in the nucleation mode (1.5–5 nm) typically encompass secondary aerosols that form by nucleation from supersaturated vapors (Section 6.3.1). These small particles grow further by the condensation of vapor and by coagulation with other particles, forming Aitken (5 nm – 0.05 μm) and accumulation mode particles (0.05–0.5 μm).

Examples of the aerosol types in the various modes, as determined from electron microscope images, are shown in Figure 6.2. One can see that anthropogenic aerosol particles, such as soot

Table 6.1 Aerosol modes with their corresponding radius ranges.

Aerosol mode	Range in radius
Nucleation mode	1.5–5 nm
Aitken mode	5 nm–0.05 μm
Accumulation mode	0.05–0.5 μm
Coarse mode	0.5–5 μm
Giant particles	> 5 μm

https://doi.org/10.1017/9781009485654.007 Published online by Cambridge University Press

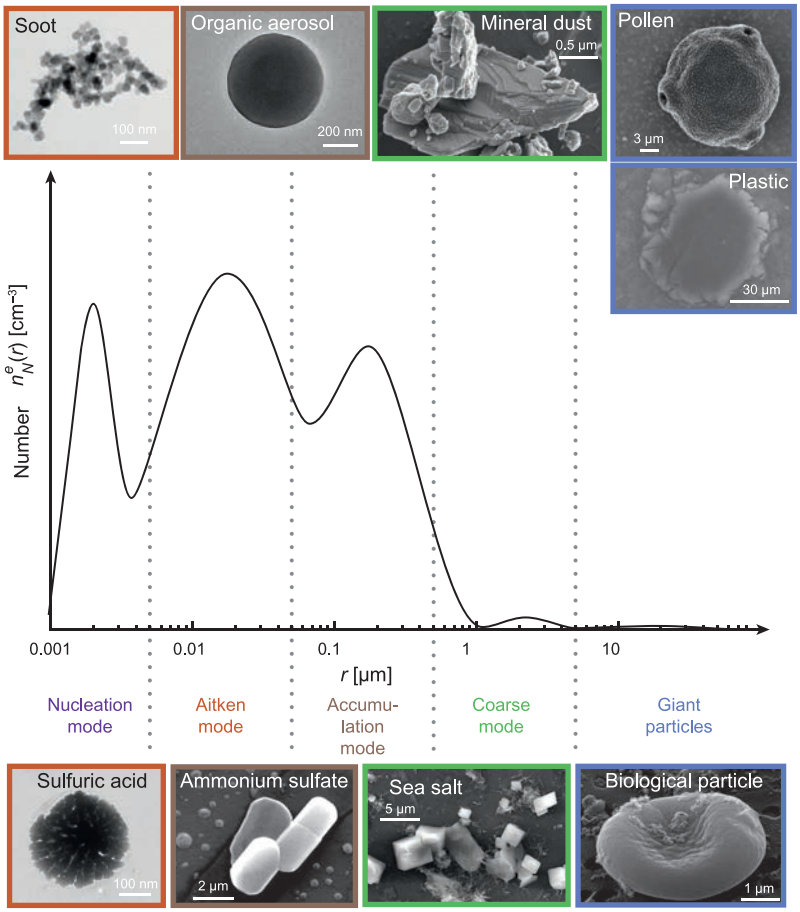


Figure 6.2 Schematic of a typical atmospheric aerosol particle number size distribution, illustrating the different modes listed in Table 6.1. Also shown are examples of different aerosol types from electron microscope images for the different aerosol modes as a function of their sizes. For each image, the scale bar provides an approximate size, and the colored outline indicates the characteristic mode in which the particle type is typically found. Photographs taken by Kouji Adachi (sulfuric acid, organic aerosol (tar ball from biomass burning), plastic particle), Martin Ebert (ammonium sulfate, sea salt, biological particle), Fabian Mahrt (soot), and by the staff of the Scientific Center for Optical and Electron Microscopy at ETH Zurich (pollen, mineral dust).

and sulfuric acid, are typically in the submicron range, while natural aerosol particles, such as mineral dust and sea salt, are typically mainly in the supermicron range. Aerosol size can easily be related to surface area, volume, or mass if either the density of the particle is known or a density is assumed.

(ii) The density of an aerosol together with its size and morphology determine its mass. The typical densities and molecular weights of some major aerosol types discussed here are

https://doi.org/10.1017/9781009485654.007 Published online by Cambridge University Press

Table 6.2 Molecular weights in g mol^{-1} and densities in kg m^{-3}, as used in the ECHAM6-HAM global climate model (GCM) and mass extinction coefficients (MECs) in m^2 g^{-1}(Gliß et al., 2021) of major aerosol types. Because ECHAM-HAM does not treat nitrate, its density was taken from Heald et al. (2014).

Aerosol type	Molecular weight	Density	MEC
Black carbon (BC)	12.01	2000	10.3
NaCl	58.44	2165	2.8
Nitrate (NO_3)	62.05	1700	5.5
Sulfate (SO_4)	96.06	1841	8.5
OA	180	2000	6.1
Mineral dust	250	2650	0.74

summarized in Table 6.2. Most aerosol types are approximately twice as dense as water, the exception being mineral dust, which is more than 2.5 times as dense as water.

(iii) The morphology of aerosols accounts for the overall geometry of the particles, including if their surfaces are rough or smooth. A liquid aerosol particle is approximately spherical, while solid aerosol particles often have complex morphologies. For example, BC particles are usually composed of primary carbon spheres that agglomerate together into aggregates with fractal morphologies (e.g., Samson et al., 1987; Adachi et al., 2007; Zhang et al., 2008), while fresh, crystalline sea salt particles often from cubic particles with sharp faces (Adachi and Buseck, 2015), see also Figure 6.2.

(iv) The phase state of the aerosol particles, whether they are liquid or solid, impacts their ability to form clouds: As we will see in Chapter 7, liquid or water-soluble particles can act as CCN and become activated to cloud droplets in warm clouds. By contrast, solid or water-insoluble aerosol particles can act as INPs and promote ice crystal formation in ice and mixed-phase clouds, as we will see in Chapter 9. An example of an aerosol type that usually exists in a liquid phase state under tropospheric conditions is sulfuric acid. By contrast, mineral dust particles exist in a crystalline, solid phase state. Note that here we specify the phase state as a *crystalline* solid, to differentiate it from an *amorphous* solid phase state. In contrast to the lattice structure of crystalline solids, amorphous solids lack long-range molecular order. In fact, OA can exist in an amorphous solid (also called *glassy*), amorphous semi-solid, or liquid phase state, which can best be described by different dynamic viscosities (Virtanen et al., 2010; Koop et al., 2011; Reid et al., 2018). For example, the term semi-solid describes materials with intermediate dynamic viscosities similar to the viscosity of peanut butter, while liquids and solids have lower and higher viscosities, respectively.

The phase state of aerosol particles can change as a function of atmospheric conditions. For example, the phase state of sea salt, or other inorganic materials such as ammonium nitrate and ammonium sulfate aerosols depends on the environmental RH. In response to changes in RH, these aerosol particles can undergo phase transitions, which results in changes to the

https://doi.org/10.1017/9781009485654.007 Published online by Cambridge University Press

particle phase state (Martin, 2000), as we will see in Section 7.3. Similarly, an OA particle can undergo phase changes between the liquid, amorphous semi-solid or amorphous solid phase state, depending on the environmental RH and temperature conditions (e.g., Renbaum-Wolff et al., 2013; Shiraiwa et al., 2017).

The phase state of aerosol particles not only impacts their ability to act as CCN or INPs, but also other atmospheric processes, such as their heterogeneous and multiphase chemical reactivity (e.g., Ravishankara, 1997; Kuwata and Martin, 2012). For example, the reactive uptake of ozone (O_3) onto OA particles can decrease with increasing particle viscosity, when the diffusion of O_3 in the bulk particle phase is slower (Shiraiwa et al., 2011). This can reduce the degradation of pollutants, that are internally mixed with OA, by O_3, with important implications for health and air pollution (Shrivastava et al., 2017).

Besides changing their phase state in response to changes in atmospheric temperature and humidity, individual aerosol particles can consist of more than one phase. A prominent example is liquid–liquid phase separation (Marcolli and Krieger, 2006). Liquid–liquid phase separation describes the phase transition from an aerosol particle with a single condensed phase to a particle with two condensed phases. It is frequently observed for particles that are internal mixtures of inorganic salts and OA (You et al., 2014; Freedman et al., 2024), but also occurs in particles that are internal mixtures of different organic materials (e.g., Mahrt et al., 2022). Whether an aerosol has one or two phases affects their atmospheric impacts, such as the equilibrium partitioning between the gas and the particle phase (Shiraiwa et al., 2013), and the ability of the particles to act as CCN (Ovadnevaite et al., 2017).

6.2 Aerosol Size Distributions

Not only the total aerosol number concentration matters, but also the particle sizes and their relative contribution to the total concentration. Therefore, we often classify the particles according to their size. These size distributions can be discrete or continuous functions. In the following, we will introduce these concepts and for simplicity make the assumption that all particles are perfectly spherical. We start by discussing aerosol size distributions in terms of particle number and then also discuss the related surface, volume, and mass distributions. Unless stated otherwise, we always refer to *number size distribution*, when discussing aerosol size distributions.

6.2.1 Discrete Size Distributions

With aerosol measurements, we obtain particle size distributions from the entire aerosol population entering the instrument. These instruments often select particles with radii in a narrow size range or bin, Δr [e.g., $r, r+\Delta r$] and measure their number concentration. By repeating this for all bins over the whole aerosol size range of the instrument, the particle number size distribution can be measured. The size distribution is then obtained by plotting the particle number concentration per size bin ΔN_i against the average radius r_i of the respective size bin. In practice, the size bins often increase with increasing radius and vary between different instruments,

https://doi.org/10.1017/9781009485654.007 Published online by Cambridge University Press

complicating the comparison of results from different measurement techniques. To obtain an instrument-independent particle size distribution, normalization of the measured number concentration in each size bin by its width is required and converting the size to an equivalent size.

Statistics can help to reduce the measured data to quantities such as arithmetic or geometric mean radius, median radius (the radius where exactly half of the particles are smaller and half of the particles are larger in size) or mode radius (the radius where the size distribution peaks), standard deviation, and total number concentration. However, information about the shape of the particle size distribution is lost if one cannot assume the sizes of the measured aerosol particles to be distributed according to a known distribution function.

6.2.2 Size Distribution Function

Decreasing the width of the discrete size bins Δr until Δr approaches dr allows us to describe the particle number distribution as a continuous function of the radius r, rather than using the discrete method introduced earlier. We can thus define the particle number density function $n_N(r)$:

$$n_N(r) = \frac{dN(r)}{dr}, \tag{6.1}$$

where $n_N(r)$ denotes the number of particles per unit volume of air within a size range of unit length around radius r. In atmospheric science, $n_N(r)$ is usually expressed in units of $\mu m^{-1}\,cm^{-3}$ (Seinfeld and Pandis, 2016). Here, 1 μm is chosen to be the unit length of the particle radius. The number density function is thus the derivative of the cumulative number distribution function $N(r)$.

The total number of particles N_a is then obtained by integrating the number density function $n_N(r)$ over the whole size range:

$$N_a = \int_0^\infty n_N(r)dr. \tag{6.2}$$

The arithmetic mean μ_a and the arithmetic standard deviation σ_a of $n_N(r)$ are given by

$$\mu_a = \frac{1}{N_a}\int_0^\infty r n_N(r)dr, \tag{6.3}$$

$$\sigma_a = \sqrt{\frac{1}{N_a}\int_0^\infty (r-\mu_a)^2 n_N(r)dr}. \tag{6.4}$$

A typical aerosol size distribution spans several orders of magnitude in particle radius and is strongly skewed toward smaller particles. Therefore, the arithmetic mean and standard deviation are usually of little practical value in summarizing the size distribution of an aerosol population. For example, a few very large particles can dominate μ_a, whereas the many very small particles do not contribute significantly. Therefore, μ_a is often significantly larger than characteristic quantities, such as median or mode radius, which give intuitive information about the "typical" radius of the aerosol under consideration. Knowledge of σ_a is useful only in combination with knowledge about μ_a because σ_a is not invariant upon scaling of the size

https://doi.org/10.1017/9781009485654.007 Published online by Cambridge University Press

axis (e.g., multiplying the radius of every particle in the distribution by a constant factor). For this reason, instead of μ_a and σ_a, the geometric mean μ_g and geometric standard deviation σ_g are generally used to summarize a particle size distribution information. For a given set of N_a particles, they are defined as follows:

$$\mu_g = exp\left(\frac{\sum_i^n n_i(r) \cdot \ln(r_i)}{N_a}\right) \tag{6.5}$$

$$\sigma_g = exp\left(\sqrt{\frac{\sum_i^n (\ln(r_i) - \ln(\mu_g))^2 \cdot n_i(r)}{N_a}}\right), \tag{6.6}$$

where the index i runs over all particles. The geometric standard deviation σ_g is invariant under scaling of the particle radii. Therefore, σ_g gives size-independent information about the width of the distribution and allows us to compare the widths of particle populations with different typical radii. A monodisperse aerosol population has $\sigma_g = 1$. In the atmosphere, the values of σ_g typically range from around 1.1 for an aerosol population with a very narrow size distribution to more than 2 for a very broad size distribution. A broad aerosol size distribution, consisting of one or more peaks or modes, is called a *polydisperse aerosol* population. By contrast, a *monodisperse aerosol* is one where all particles are of the same size. For monodisperse aerosol, $\mu_a = \mu_g$, otherwise $\mu_g < \mu_a$.

A further consequence of the large size range and the asymmetry of atmospheric particle size distributions is that the distribution function $n_N(r)$ as defined in eq. (6.1) presents difficulties in visualizing the overall features of the size distribution. For most aerosol populations, a sharp peak at small particle sizes is followed by a long, hardly visible tail. As an example, consider a distribution $n_N(r)$ with a peak at 20 nm. The number concentration of particles falling into a 10 nm size bin around 200 nm is negligible compared with the number concentration of particles in a 10 nm size bin around 20 nm. Nevertheless, the presence of a few large particles can be highly important for atmospheric processes such as cloud droplet formation (Chapter 7) or ice nucleation (Chapter 9). A better representation of large particles in the tail of the distribution can be achieved if the distribution function is normalized to unit size bins on a logarithmic length scale instead of a linear length scale, as shown in Figure 6.3a.

This leads to the commonly used distribution function

$$n_N^e(r) = \frac{dN}{d\ln r} = \frac{dN}{dr}\frac{dr}{d\ln r} = r n_N(r), \tag{6.7}$$

with units cm^{-3}. $n_N^e(r)$ gives the number concentration of particles around radius r in a size bin of unit length on a logarithmic scale. In a log-normal distribution, the logarithm of r is normally distributed.

Mathematically, only $n_N(r)$ is a log-normal distribution, whereas $n_N^e(r)$ is skewed by multiplying the log-normal distribution by radius. However, in atmospheric science, both $n_N(r)$ and $n_N^e(r)$ are referred to as log-normal distributions. Size distributions referring to unit length on a logarithmic scale correspond to exponentially increasing size bins on a linear length scale. For example, using base 10 for the logarithms, a size bin of unit length on the logarithmic scale ranges over 90 nm, from 10 to 100 nm, but over 9 μm from 1 to 10 μm for large particles. Both size distributions, $n_N(r)$ and $n_N^e(r)$, have advantages: An advantage of the use of

https://doi.org/10.1017/9781009485654.007 Published online by Cambridge University Press

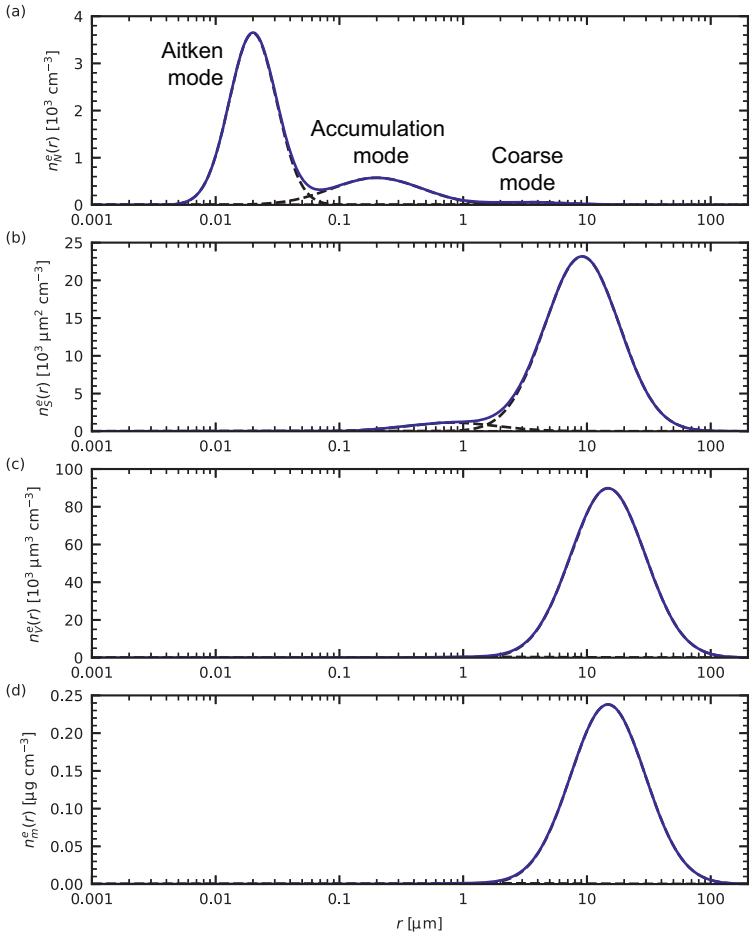


Figure 6.3 (a) Number, (b) surface, (c) volume, and (d) mass size distributions, as obtained from eqs. (6.10)–(6.13). In each panel, the solid, colored line denotes the sum of three individual log-normal distributions (dashed lines) given by $N_{a,1} = 4000\,\mathrm{cm}^{-3}$, $\sigma_{g,1} = 1.55$, $\mu_{g,1} = 0.02\,\mu\mathrm{m}$; $N_{a,2} = 1200\,\mathrm{cm}^{-3}$, $\sigma_{g,2} = 2.3$, $\mu_{g,2} = 0.2\,\mu\mathrm{m}$; $N_{a,3} = 100\,\mathrm{cm}^{-3}$, $\sigma_{g,3} = 2$, and $\mu_{g,3} = 3.5\,\mu\mathrm{m}$. For the mass distribution, an aerosol material density of $\rho = 2650\,\mathrm{kg\,m}^{-3}$ was used.

$n_N^e(r)$, on the one hand, is that its values do not depend on the choice of a unit for the length scale. In contrast, the value of $n_N(r)$ changes if 1 nm is chosen as the width of the unit size bin instead of 1 µm. An advantage of $n_N(r)$, on the other hand, is that the area below the curve is proportional to the total particle number concentration, which is not the case for $n_N^e(r)$.

6.2.3 Logarithmic Normal Size Distributions

In general, an atmospheric aerosol population can be described reasonably well either by a single log-normal size distribution or by a linear superposition of such distributions (Whitby and Sverdrup, 1980), where each distribution is given by

https://doi.org/10.1017/9781009485654.007 Published online by Cambridge University Press

$$n_N^e(r) = \frac{dN}{d\ln r} = \frac{N_a}{\sqrt{2\pi}\tilde{\sigma}_a} \exp\left[\frac{-(\ln r - \tilde{\mu}_a)^2}{2\tilde{\sigma}_a^2}\right]. \tag{6.8}$$

Here, $\tilde{\mu}_a$ is the arithmetic mean of the logarithms of the particle radii. This is the same as the logarithm of the geometric mean aerosol radius, $\tilde{\mu}_a = \ln \mu_g$ (eq. 6.5). The standard deviation of $\ln r$ is given by

$$\tilde{\sigma}_a = \sqrt{\frac{1}{n}\sum_i (\ln r_i - \ln \mu_g)^2}. \tag{6.9}$$

Comparison with eq. (6.6) shows that $\tilde{\sigma}_a = \ln \sigma_g$. Hence, the number distribution of a typical aerosol population can be written as

$$n_N^e(r) = \frac{dN}{d\ln r} = \frac{N_a}{\sqrt{2\pi}\ln \sigma_g} \exp\left[\frac{-(\ln r - \ln \mu_g)^2}{2\ln^2(\sigma_g)}\right]. \tag{6.10}$$

There are some points that are worthwhile to note about log-normal particle number distributions, as follows:

- The median radius of a log-normal number distribution is equal to the geometric mean radius μ_g.
- In a log-normal number distribution, 68 % of all particles lie in the range μ_g/σ_g to $\mu_g\sigma_g$ and 95 % of all particles lie in the range μ_g/σ_g^2 to $\mu_g\sigma_g^2$.
- An aerosol population with a narrow size distribution can also be described by a normal distribution, since the skewness of a log-normal distribution decreases with decreasing σ_g, that is, the log-normal distribution approaches a normal distribution.
- The distribution function remains the same up to a constant factor upon a change in the base of the logarithm, for example, $\ln(r) = \log_{10}(r) \cdot 2.3025$.

In an aerosol population, each of the five modes introduced in Section 6.1.2 is represented by an individual log-normal size distribution, and the source strength as well as the history of the aerosol in the atmosphere determine to which extent each mode contributes to the total size distribution.

6.2.4 Surface, Volume, and Mass Size Distributions

So far, we have characterized aerosol populations only in terms of their number size distribution. However, other aerosol characteristics, such as surface and volume, are important as well, depending on the atmospheric process of interest. For instance, number distributions are of interest when the ability of the aerosol particles to act as CCN (Chapter 7) or INPs (Chapter 9) is studied. Surface distributions are relevant when one is investigating the radiative properties of aerosol particles since the surface area of an aerosol particle determines the amount of solar radiation that it scatters (Section 12.1). The surface distribution is also important in terms of chemistry, as the uptake of molecules on the surface of aerosol particles strongly depends on the available surface area (Moise and Rudich, 2000; Ammann et al., 2003).

https://doi.org/10.1017/9781009485654.007 Published online by Cambridge University Press

Volume or mass distributions are used to obtain information about the aerosol burden in the atmosphere. Here, *aerosol burden* refers to the vertically integrated aerosol mass mixing ratio, that is, the ratio of the mass of a given particle type in a given volume to the total mass of air in that volume. The amount of radiation absorbed by aerosol particles that are much smaller than the wavelength of the incident light is proportional to the particle volume, and mass (Moosmüller et al., 2009).

Recalling that the surface of a sphere is given by $S = 4\pi r^2$ and the volume by $V = (4/3)\pi r^3$, we can compute surface, volume, and mass distribution functions based on eq. (6.10) from:

$$n_S^e(r) = \frac{dS}{d\ln r} = 4\pi r^2 n_N^e(r) = 4\pi r^2 \frac{N_a}{\sqrt{2\pi}\ln\sigma_g} \exp\left[\frac{-(\ln r - \ln\mu_g)^2}{2\ln^2(\sigma_g)}\right], \tag{6.11}$$

$$n_V^e(r) = \frac{dV}{d\ln r} = \frac{4}{3}\pi r^3 n_N^e(r) = \frac{4}{3}\pi r^3 \frac{N_a}{\sqrt{2\pi}\ln\sigma_g} \exp\left[\frac{-(\ln r - \ln\mu_g)^2}{2\ln^2(\sigma_g)}\right], \tag{6.12}$$

$$n_m^e(r) = \frac{dm}{d\ln r} = \frac{4}{3}\pi r^3 \rho n_N^e(r) = \frac{4}{3}\pi r^3 \rho \frac{N_a}{\sqrt{2\pi}\ln\sigma_g} \exp\left[\frac{-(\ln r - \ln\mu_g)^2}{2\ln^2(\sigma_g)}\right], \tag{6.13}$$

where ρ is the material density of the aerosol particles. $n_S^e(r)$ is given in $\mu m^2\,cm^{-3}$, $n_V^e(r)$ in $\mu m^3\,cm^{-3}$ and $n_m^e(r)$ in $g\,cm^{-3}$.

Figure 6.3 shows the number, surface, volume, and mass distributions of an aerosol population, using eqs. (6.10)–(6.13). The solid curve in Figure 6.3a denotes the number distribution of all aerosol particles in this population, which consists of a superposition of three individual log-normally distributed modes. The number size distribution peaks at $\approx 0.02\,\mu m$ in the Aitken mode, with smaller modes at 0.2 μm in the accumulation mode and 3.5 μm in the coarse mode (Table 6.1). In general, atmospheric aerosol distributions can often be described as the sum of three or four log-normal distributions, depending on the source of the particles (Whitby and Sverdrup, 1980).

It is worth noting that the number, surface, and volume distributions depicted in Figure 6.3 differ in terms of the modes that dominate each distribution. While the number distribution shows the highest abundance for Aitken mode particles, the surface and volume distributions are dominated by coarse mode particles, which are hardly visible in the number size distribution.

The surface, volume, and mass distributions defined in eqs. (6.11)–(6.13) are no log-normal distributions. However, they can be transformed into log-normal distributions by employing surface, volume, and mass geometric mean radii $\mu_{g,S}$, $\mu_{g,V}$, and $\mu_{g,m}$, respectively:

$$\ln\mu_{g,S} \equiv \frac{\sum s_i \ln r_i}{S_a} = \ln\mu_g + 2\ln^2\sigma_g, \tag{6.14}$$

$$\ln\mu_{g,V} \equiv \frac{\sum v_i \ln r_i}{V_a} = \ln\mu_g + 3\ln^2\sigma_g, \tag{6.15}$$

$$\ln\mu_{g,m} \equiv \frac{\sum m_i \ln r_i}{m_a} = \ln\mu_g + 3\ln^2\sigma_g. \tag{6.16}$$

https://doi.org/10.1017/9781009485654.007 Published online by Cambridge University Press

Table 6.3 Values of the factor *b* needed for the Hatch–Choate conversion eq. (6.17), of number geometric mean radius to other average radii (Hinds and Zhu, 2022).

μ_X	b
Mass median radius or mass geometric mean radius $\mu_{g,m}$	3
Mass arithmetic mean radius $\mu_{a,m}$	3.5
Surface median radius or surface geometric mean radius $\mu_{g,S}$	2
Surface arithmetic mean radius $\mu_{a,S}$	2.5
Volume median radius or volume geometric mean radius $\mu_{g,V}$	3
Volume arithmetic mean radius $\mu_{a,V}$	3.5
Number mode radius $\widetilde{\mu}$	−1
Number arithmetic mean radius μ_a	0.5
Radius of average mass $r_{\bar{m}}$	1.5

Here, r_i, s_i, v_i, and m_i denote radius, surface, volume, and mass of the ith particle, where i runs over all particles in the aerosol population, and S_a, V_a, and m_a denote the total particle surface, volume, and mass, respectively. In contrast with the number mean radius (geometric or arithmetic), the surface mean radius is the mean over all particle radii, each weighted according to the particle surface at that particle radius. For a log-normally distributed particle population, the surface geometric mean radius, or median surface radius, $\mu_{g,S}$, denotes the radius below which half of the particle surface area is found. Analogous definitions hold for the median values of volume $\mu_{g,V}$ and mass $\mu_{g,m}$. The quantities $\mu_{g,S}$ and $\mu_{g,V}$ are larger than μ_g, since the weight of the large particles is larger in the surface and volume distributions than in the number size distribution.

A powerful property of log-normal distributions is that for a given sample, the value of σ_g is the same for all types of distributions – number, surface, volume, and mass. This allows us to calculate all the characteristic average radii μ_X for any moment (e.g., surface, volume, mass) of the distribution from only the number geometric mean radius and the universal geometric standard deviation. This can be done using the Hatch–Choate conversion equation (Hatch and Choate, 1929):

$$\mu_X = \mu_g \exp\left(b \ln^2 \sigma_g\right). \tag{6.17}$$

Here, b is a constant that only depends on the type of conversion. The values of the factor b for some average radii μ_X are given in Table 6.3 (Hinds and Zhu, 2022).

6.2.5 Observed Atmospheric Aerosol Size Distributions

Examples of size, surface, and volume distributions for a biomass-burning aerosol and a marine aerosol observed at Earth's surface are shown in Figure 6.4. The average distributions of the biomass-burning aerosol, which typically contains BC, *brown carbon* (BrC), and OA, were obtained from more than 8000 size distributions measured in the Amazon basin in

https://doi.org/10.1017/9781009485654.007 Published online by Cambridge University Press

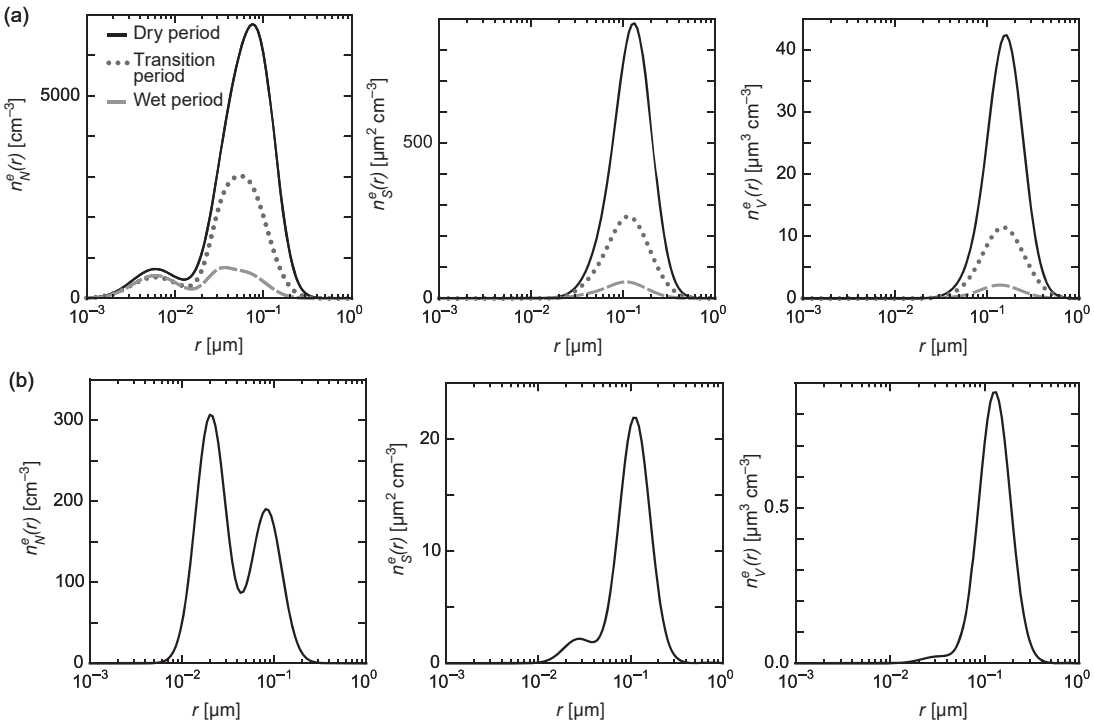


Figure 6.4 Number distribution, $n_N^e(r) = dN/d\ln r$, surface distribution, $n_S^e(r) = dS/d\ln r$ and volume distribution, $n_V^e(r) = dV/d\ln r$, as functions of the aerosol radius for (a) a biomass burning aerosol (Rissler et al., 2006) and (b) a submicron aerosol distribution found over the ocean (Heintzenberg et al., 2000). Note the differing vertical scales.

different meteorological conditions (dry period, transition period, and wet period) by Rissler et al. (2006). In all periods, the average distribution is a superposition of three log-normal distributions with contributions from the nucleation, Aitken, and accumulation modes. The highest concentrations are found in the dry period with more than 10 000 particles cm^{-3} in the accumulation mode when biomass-burning emissions are highest. They are lowest during the wet season, with less than 2000 particles cm^{-3}, when only little biomass burning takes place and aerosol particles are efficiently removed by wet deposition (Section 6.4.1).

The number concentration for the nucleation mode as well as the mode radius of the number distribution remains almost the same for the different periods. The Aitken and accumulation mode radii increase by around 50 % from the wet season to the dry season. Similarly, the number concentrations in the Aitken and accumulation modes increase by factors of 13 and 7, respectively. The distinction between the Aitken and accumulation mode is not clearly visible as their mode radii are only about a factor of 2 apart. In contrast, the nucleation mode radius, 12 nm, is a factor 5 to 8 smaller than that for the Aitken mode. The contribution of the nucleation mode vanishes in the surface and volume distributions. Likewise, the particles contributing most to the volume distribution are not visible in the number size distribution.

https://doi.org/10.1017/9781009485654.007 Published online by Cambridge University Press

Figure 6.4b shows near-global average distributions of aerosol sampled over the ocean as compiled from various ship observations (Heintzenberg et al., 2000). The average distributions are bimodal, with the larger number concentration in the Aitken mode and the secondary peak in the accumulation mode. The large Aitken mode in the size distribution reveals that the aerosol sample from the ocean has contributions from anthropogenic sources, because it includes data taken in coastal regions. The number concentration of roughly 750 cm^{-3} for the Aitken mode is, however, considerably smaller than the number concentration of the biomass-burning aerosol. The Aitken mode of the aerosol over the ocean is still visible in the surface distribution but becomes negligible in the volume distribution.

6.3 Aerosol Sources and Emissions

Emissions of aerosol particles vary according to their geographical origin. Depending on their origin, aerosols are often classified as desert, marine, polar, remote continental (referring to the continental aerosol away from big cities), urban, and free tropospheric aerosols. The free troposphere refers to the troposphere above the PBL. Biomass burning aerosols are a strong contributor to free tropospheric aerosols (Schill et al., 2020). Most aerosol types (anthropogenic aerosols, dust, sea salt) have their sources near the surface such that aerosol number and mass concentrations typically decay with altitude (e.g., Watson-Parris et al., 2019).

6.3.1 Formation Mechanisms of Aerosol Particles

Aerosol particles have a variety of different formation mechanisms. Accordingly, they are often broadly classified into primary and secondary particles. Primary particles are emitted directly as particulate matter into the atmosphere. They are to be distinguished from secondary aerosols, which form within the atmosphere from the oxidation of precursor gases, followed by gas-to-particle partitioning of the lower volatility oxidation products.

Formation of Primary Aerosol Particles

Primary aerosol particles can originate from *bulk-to-particle conversion*, such as wind-blown dust from arid regions (Claquin et al., 1999; Prospero et al., 2002; Engelstaedter et al., 2006). Bulk-to-particle conversion refers to aerolization of particles from a large (bulk) surface. Emissions of mineral dust from arid regions depend on wind speed, soil moisture, and the bare soil fraction (Tegen, 2003). The emissions of pollen and fungal spores by plants and soil are other examples of primary aerosol sources. Combustion processes can also emit considerable amounts of primary aerosol particles. For example, BC emitted as a by-product of incomplete combustion processes is often considered as primary aerosols.

Sometimes, *liquid-to-particle conversion* is distinguished from bulk-to-particle conversion. Sea salt aerosols are an example of liquid-to-particle conversion because they originate from drops ejected into the air when air bubbles in breaking waves burst at the ocean surface (e.g.,

https://doi.org/10.1017/9781009485654.007 Published online by Cambridge University Press

Lewis and Schwartz, 2004). When a sea water droplet then evaporates in the atmosphere, it leaves a sea salt particle behind. The higher the wind speed, the more sea salt aerosols are emitted, because of more wave breaking.

Formation of Secondary Aerosol Particles

Secondary particles result from the nucleation of a new phase (the condensed or particle phase) from a supersaturated gas phase with subsequent growth of the resulting aerosol particles (Zhang et al., 2012). This process is also referred to as *gas-to-particle conversion*. The most common form of new particle formation by nucleation is *binary nucleation*, where the particle phase forms from two different gas-phase precursors (chemical species). Homogeneous homomolecular nucleation from the gas phase, which is the self-nucleation of a single species, does not take place in the atmosphere, as that would require the gas phase to be supersaturated with respect to this single species alone. By contrast, for binary nucleation to take place, the gas phase can be subsaturated with respect to each individual species, while it is supersaturated with respect to their mixture. This is because in such a two- or multi-component system, the thermodynamic phase equilibria are altered compared to single-component systems (Bilde et al., 2015). The details of this reduction in vapor pressure of the mixture can be understood in the context of Raoult's law (Gaman et al., 2004), which will be discussed in Section 7.4.

A prominent example of binary nucleation is the reaction of n moles of water vapor, $H_2O(g)$, with m moles of gaseous sulfuric acid, $H_2SO_4(g)$, which itself is produced from gas-phase oxidation of SO_2 (Kulmala and Laaksonen, 1990; Brock et al., 1995). Here, n and m are arbitrary numbers. This reaction can result in the formation of a sulfuric acid cluster that, upon reaching a critical size, can nucleate into an aqueous sulfuric acid particle:

$$n\,H_2O(g) + m\,H_2SO_4(g) \rightarrow (H_2O)_n(H_2SO_4)_m(aq). \tag{6.18}$$

Here, the subscript "aq" is used to denote the considerable amount of water in these particles. This reaction leads to new particle formation in the upper troposphere, where the nucleation rate can exceed 1 particle $cm^{-3}\,s^{-1}$ (Lucas and Prinn, 2003). New particle formation is thought to contribute also to the formation of CCN (Gordon et al., 2017; Williamson et al., 2019).

The entire process from cluster formation to aerosol nucleation, with subsequent growth to larger sizes and finally activation into a cloud droplet, is shown schematically in Figure 6.5. The first step is that, in the gas phase, molecules of H_2O and H_2SO_4 form a cluster. Once the cluster exceeds a critical size, nucleation occurs (Section 7.1) and a stable sulfuric acid aerosol particle is formed. The critical size of a cluster is the size above which it is more likely for the cluster to keep growing rather than to shrink and evaporate. Once the initial (liquid) particle phase has nucleated, further gaseous species can condense onto the particle and contribute to its growth, if the gas phase is supersaturated with respect to this species. In addition, other species present in the gas phase such as organic vapors can partition from the gas phase to the particle phase and contribute to its growth (Kulmala, 2003; Tröstl et al., 2016; Hu et al., 2018). The gas-particle partitioning of organics can be described by the fundamental concepts of absorptive partitioning, where the partitioning of a given species between the gas and the

https://doi.org/10.1017/9781009485654.007 Published online by Cambridge University Press

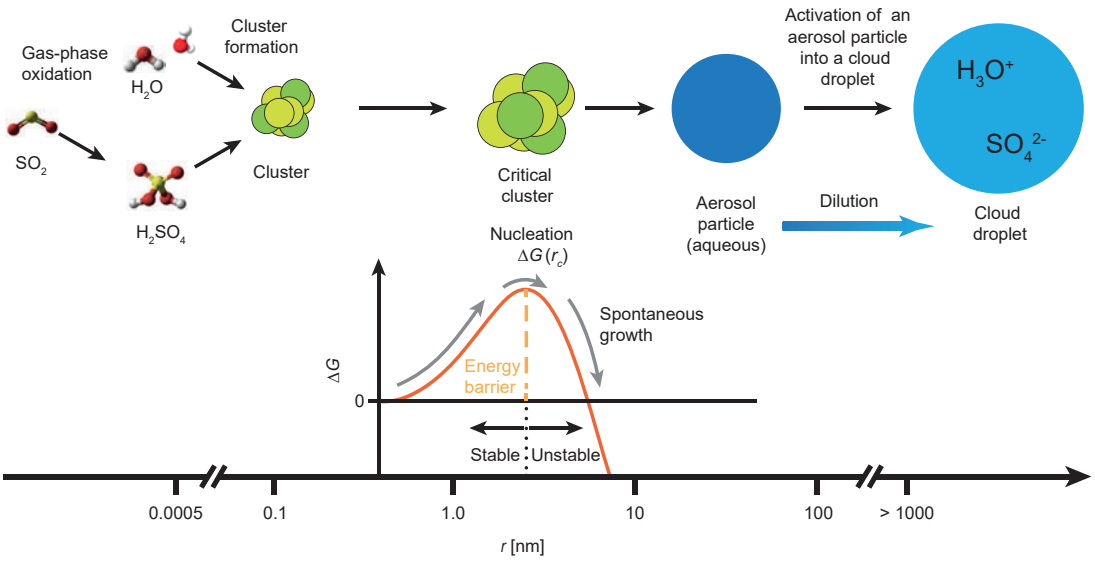


Figure 6.5 Schematic representation of the nucleation and subsequent growth process for the atmospheric binary homogeneous nucleation of H_2SO_4(g) and H_2O(g). Once stable clusters are formed, other substances can take part in the growth process. Particles may grow to sizes large enough to activate into cloud droplets.

particle phase is described by an equilibrium partitioning coefficient or the saturation vapor concentration of that species (Pankow, 1994; Odum et al., 1996; Donahue et al., 2006).

The ambient concentrations of H_2SO_4(g) and H_2O(g) are too low to explain the observed nucleation rates in the PBL (Sipilä et al., 2010) by the simple binary nucleation considered above. While sulfuric acid likely plays a key role for the formation of clusters upon which new particles are formed, ions produced by galactic-cosmic rays (Kirkby and et al., 2011), low-volatility organic vapors (Ehn et al., 2014; Riccobono et al., 2014; Stolzenburg et al., 2018), and other ternary species such as ammonia (NH_3) and amines (Kirkby and et al., 2011; Almeida et al., 2013) can help to stabilize the initial cluster and decrease evaporation (Kirkby et al., 2023). While observing new particle formation down to the scale of molecular clusters is a challenge for available measurement techniques, computational methods can provide valuable insights into the formation and growth of atmospheric molecular clusters (Elm et al., 2020).

An important type of secondary aerosol particles is the *secondary organic aerosol* (SOA). SOA particles mostly form from the oxidation of organic precursors gases, so-called *volatile organic compounds* (VOCs) (Hallquist et al., 2009). SOA precursors are emitted from both anthropogenic and biogenic sources (Kanakidou et al., 2005), with the latter dominating SOA formation globally (Spracklen et al., 2011). The most important classes of biogenic SOA precursors are isoprene (C_5) (Claeys et al., 2004), monoterpenes (C_{10}) (Ehn et al., 2014), and sesquiterpenes (C_{15}) (Yee et al., 2018), emitted from vegetation. An important class of anthropogenic SOA precursors are aromatic compounds, examples of which include toluene or naphthalene, which are often emitted during combustion processes. The reaction of these organic vapors with atmospheric oxidants, including ozone (O_3), hydroxyl radicals (OH), and

https://doi.org/10.1017/9781009485654.007 Published online by Cambridge University Press

nitrate radicals (NO_3), leads to oxidation products with lower volatility, ultimately resulting in the gas-to-particle partitioning of these products, and the formation of SOA particles.

The *volatility* describes the partitioning of a compound between the vapor and the particle phase, and is an important property of atmospheric OA (Donahue et al., 2006). The volatility of any (organic) compound is determined by its saturation vapor pressure and its condensed phase concentration. In atmospheric science, it is common to express the volatility as an (effective) saturation mass concentration in units of $\mu g\,m^{-3}$ (Donahue et al., 2011), describing the concentration of the component in the gas phase. Substances with a low volatility, that is, a low saturation concentration and a low saturation vapor pressure, preferentially partition to the particle phase (Bilde et al., 2015). Conversely, components with a high volatility, that is, a high saturation concentration and high saturation vapor pressure, preferentially partition to the gas phase.

Formation of new (secondary) aerosol particles by nucleation usually takes place when the background aerosol number concentration is low. Then, the existing total aerosol surface area is too small for the condensable vapors to condense onto these surfaces. Instead, they accumulate in the gas phase, become supersaturated and eventually nucleation of new, secondary particles occurs. A typical example of an aerosol nucleation event, as observed in a boreal forest in Finland, is shown in Figure 6.6 (Boy and Kulmala, 2002). Here, new particle formation

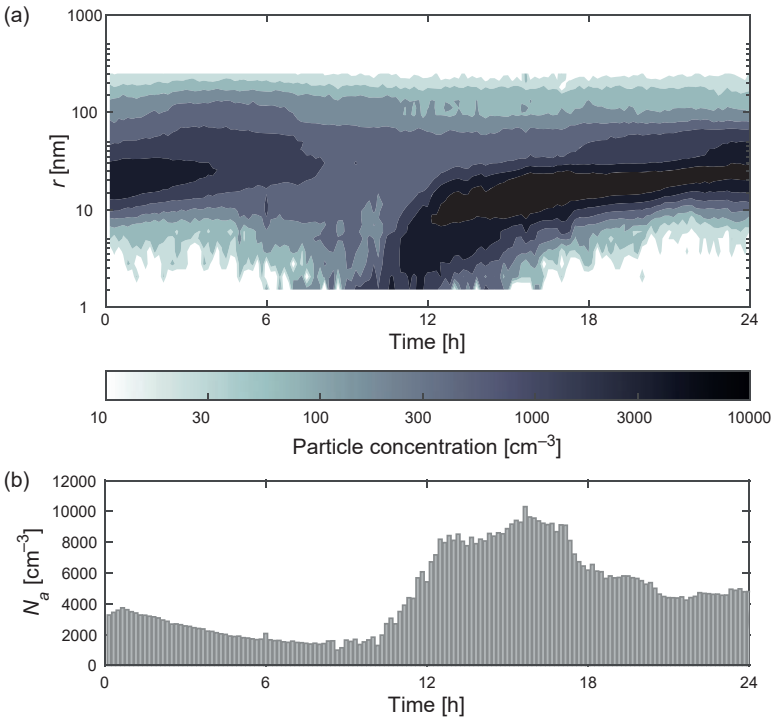


Figure 6.6 Example of a typical gas-to-particle nucleation event as a function of time as observed in Hyytiälä, Finland, on May 19, 1999: (a) particle number size distribution, (b) total number concentration. Figure adapted from Boy and Kulmala (2002).

https://doi.org/10.1017/9781009485654.007 Published online by Cambridge University Press

by nucleation set in at around 9:00 local time, as can be seen in the strong increase in particle number concentration of the smallest aerosol particles. Until 13:00 local time, new particles were formed and grew rapidly in size. Thereafter, the total particle number concentration remained approximately constant, until around 17:00 local time. During that time period, the particles still continued to grow, albeit at a lower rate. A key class of VOCs that is emitted from vegetation (pine trees) in these boreal environments are monoterpenes, including α-pinene ($C_{10}H_{16}$). Once released in the atmosphere, the α-pinene vapors become oxidized and form SOA particles. The formation of new particles in Figure 6.6 takes place during daytime, suggesting that this new particle formation is driven by photochemical oxidation, with OH being a major daytime oxidant for VOCs.

The contours of a new particle formation and growth event in the aerosol number size distribution over time (like in Figure 6.6a) often resemble the shape of a banana and are thus sometimes referred to as a "banana plot". New particle formation has been observed at many different locations globally. For instance, it can also take place in polluted regions such as urban centers, provided that the concentration of the condensable vapors is sufficiently high to not only condense onto the pre-existing aerosol surfaces (e.g., Kerminen et al., 2018; Xiao et al., 2021).

6.3.2 Aerosol Emissions

In order to estimate the transport of aerosol particles and their influence on air quality and climate, knowledge about the spatial distribution of aerosol emissions is needed. Aerosol particles have a high variability in both space and time compared to long-lived GHGs, which are well-mixed throughout the atmosphere. The global emission rates of major aerosol types, their burdens, and lifetimes are summarized in Table 6.4. The lifetime of an aerosol type is calculated from its global mean burden divided by its emission rate.

Table 6.4 Global emission rates, burdens, and lifetimes of major aerosol types for the year 2010. The median values and inter-model standard deviations of the emissions, lifetimes, and burdens are taken from an aerosol model intercomparison (Gliß et al., 2021). The sources of OA are classified into primary organic aerosol (POA) and secondary organic aerosol (SOA), but the uncertainty estimate is only available for OA.

Aerosol type	Emission rate (Tg yr^{-1})	Burden (Tg)	Lifetime (d)
Primary emissions			
Sea salt	4980.000 ± 12.190	8.7 ± 5.6	0.6 ± 0.8
Mineral dust	1440 ± 1174	16.6 ± 5.1	3.7 ± 1.6
POA	74.6		
BC	9.7 ± 0.4	0.13 ± 0.06	5.5 ± 2.1
Secondary emissions			
SO_4	143 ± 47	1.80 ± 0.75	4.9 ± 1.5
SOA	41.4		
NO_3	32.5 ± 51.3	0.17 ± 0.36	3.9 ± 3.2
Total OA	116.0 ± 52.9	1.90 ± 0.68	6.0 ± 1.8
Sum of all types	6721.2	27.4	

https://doi.org/10.1017/9781009485654.007 Published online by Cambridge University Press

The emission data in Table 6.4 were compiled from 14 global climate model (GCM) simulations of the aerosol intercomparison project (AEROCOM) (Gliß et al., 2021) and are representative for the year 2010. Emission inventories collect or estimate emission data for various countries and aerosol compounds from various sectors, such as biomass-burning and industrial activities. The emission rates of mineral dust and sea salt particles depend on wind speed and are calculated directly within the models. The AEROCOM emission data set used in Gliß et al. (2021) distinguishes natural and anthropogenic emissions of major aerosol types, sea salt, mineral dust, sulfate, nitrate, BC, and OA. Aerosol precursors provided only by a few of the models, such as NO_x, NH_4^+, and VOC, are not analyzed. Furthermore, aerosol types that are associated with large uncertainties, such as bacteria, fungal spores, or pollen are not included in AEROCOM.

Geographical distributions of the annual mean emissions averaged over the decade 2003–2012 from different aerosol sources are shown in Figure 6.7. Mineral dust and sea salt are the two most abundant aerosol types in terms of mass. They originate from bulk-to-particle and liquid-to-particle conversion, respectively, and are therefore primary particles. Sea salt has the largest emission rate with almost $5000\,\mathrm{Tg\,yr^{-1}}$ (Table 6.4). The main sources of sea salt aerosols are the oceans in the west-wind zones, the Roaring Forties in the Southern Hemisphere and the storm tracks over the North Atlantic and North Pacific Ocean. Mineral dust has the second largest emission rate and is mainly a natural aerosol that is produced through wind erosion in sparsely vegetated and arid regions. Globally, the most important dust sources are deserts, especially the Sahara and Gobi deserts. Because the regions that emit mineral dust are much smaller than the source regions of sea salt, the global emissions of mineral dust amount to only about $1440\,\mathrm{Tg\,yr^{-1}}$. The other aerosol types displayed in Figure 6.7 are dominated by anthropogenic emissions (BC, primary organic aerosol (POA) and sulfate), but also have natural sources from, for example, wild fires (Kondo et al., 2011), as detailed later.

Only about 2.5% of the sulfate aerosols are directly emitted as particulate matter. The majority of the sulfate aerosols is formed by gas-to-particle conversion from the oxidation of sulfur dioxide (SO_2) either in the gas phase or within cloud droplets (Fig. 6.5). SO_2 is emitted from both biogenic and anthropogenic sources. The anthropogenic SO_2 emissions can further be subdivided into individual sectors (van Marle et al., 2017; Hoesly et al., 2018). For the year 2010, these encompass emissions from energy production ($48.1\,\mathrm{Tg\,yr^{-1}}$), industry ($36.6\,\mathrm{Tg\,yr^{-1}}$), shipping ($10.9\,\mathrm{Tg\,yr^{-1}}$), residential, commercial, and other emissions ($6.7\,\mathrm{Tg\,yr^{-1}}$), transportation ($3\,\mathrm{Tg\,yr^{-1}}$), biomass burning ($2.2\,\mathrm{Tg\,yr^{-1}}$), and waste ($0.2\,\mathrm{Tg\,yr^{-1}}$). Natural sources of SO_2 include emissions of volcanoes. Even though explosive volcanic eruptions emit a lot of SO_2 at once, major explosive eruptions are rare events. Therefore, the volcanic SO_2 emissions are dominated by those from continuously outgassing volcanoes with $23.2\,\mathrm{Tg\,yr^{-1}}$ (Carn et al., 2017) as compared with only $2.4\,\mathrm{Tg\,yr^{-1}}$ from explosive volcanoes averaged over the 40-year period 1979–2018.

There are also other natural sources of sulfate, for example, some phytoplankton species emit dimethyl sulfide (DMS) when they die, which is the most abundant biological sulfur source in the marine atmosphere (Andreae et al., 1985; Bates et al., 1992). Once emitted, DMS is oxidized within the atmosphere to methane sulfonic acid (MSA), SO_2, and other species (Barnes et al., 2006; Veres et al., 2020) and can contribute to new particle formation (Rosati et al., 2021). SO_2 is then further oxidized to SO_4^{2-} (sulfate). In the year 2000, DMS

https://doi.org/10.1017/9781009485654.007 Published online by Cambridge University Press

emissions amounted to 18.2 Tg yr^{-1} (Dentener et al., 2006). There is also a small terrestrial source of DMS from vegetation, which is less than 2% of the oceanic DMS source (Pham et al., 1995).

The map of sulfur emissions in Figure 6.7a encompasses DMS, SO_2, and sulfate. The major shipping lanes are visible because ships could burn sulfur-rich fuel outside of emission controlled areas (ECAs) before the fuel sulfur regulations of the International Maritime Organization 2020 were put in place (Diamond, 2023). As compared with the SO_2 emissions from ships, aircraft emissions of SO_2 are negligible (Skeie et al., 2009). Relative sulfur emission maxima over the oceans are related to DMS emissions. The highest emissions over land are associated mainly with fossil fuel combustion and occur predominantly in southeast Asia, Europe, and North America.

Emissions of carbonaceous aerosol particles are subdivided into OA (sum of POA and SOA in Figure 6.7c) and BC (Figure 6.7d). BC originates from primary emissions, whereas OA is often further subdivided into POA and SOA. The relative contribution of POA and SOA to the total OA remains a matter of ongoing debate, with previous studies reporting different estimates (Kanakidou et al., 2005; Hallquist et al., 2009; Jimenez et al., 2009). Discerning the relative contributions of POA and SOA to the total OA is complicated for a number of reasons. For instance, in the atmosphere, dilution of POA plumes with environmental air masses can cause evaporation of some POA, causing re-partitioning of the organic compounds to the gas phase. If these species then undergo chemical transformations in the gas phase, they can become (further) oxidized to species with sufficiently low volatility, which can then partition back to the particle phase and contribute to SOA (Palm et al., 2020). Similarly, condensed (particle) phase oxidation of POA to form SOA can influence the relative contribution to total OA. Thus, while the classification of OA into POA and SOA provides an intuitive means to distinguish the various types of organic aerosols, this classification can be ambiguous and thus should only be considered as a first-order categorization.

Although biomass burning from wildfires plays a minor role for SO_2 emissions, it is an important source of BC, POA, and gaseous species that can lead to the formation of SOA (Andreae, 2019; Decker et al., 2021) (Figures 6.7b, c). This is due to the often incomplete combustion of biomass, as complete combustion would produce only CO_2 and H_2O. The relative amounts of BC and POA emitted during combustion depend on the availability of oxygen. Less oxygen being available for combustion leads to less complete combustion and to higher amounts of BC. Because oxygen is always available in the atmosphere but not in sufficient amounts at the emission source, BC is always emitted together with POA, so that these two emission maps look rather similar.

For the year 2010, the POA emissions were dominated by anthropogenic emissions from biomass burning (22.1 Tg yr^{-1}), residential, commercial, and other sources (12.2 Tg yr^{-1}), fossil fuel combustion (4.9 Tg yr^{-1}), and waste (2.2 Tg yr^{-1}) amounting to 41.4 Tg yr^{-1} of POA in total (van Marle et al., 2017; Hoesly et al., 2018). A considerable fraction of atmospheric POA can be classified as hydrocarbon-like organic aerosol (HOA) (Jimenez et al., 2009). For example, primary particles from engine lubricating oil associated with vehicle exhaust have been found to be a major component of HOA (Collier et al., 2015). The global annual mean

https://doi.org/10.1017/9781009485654.007 Published online by Cambridge University Press

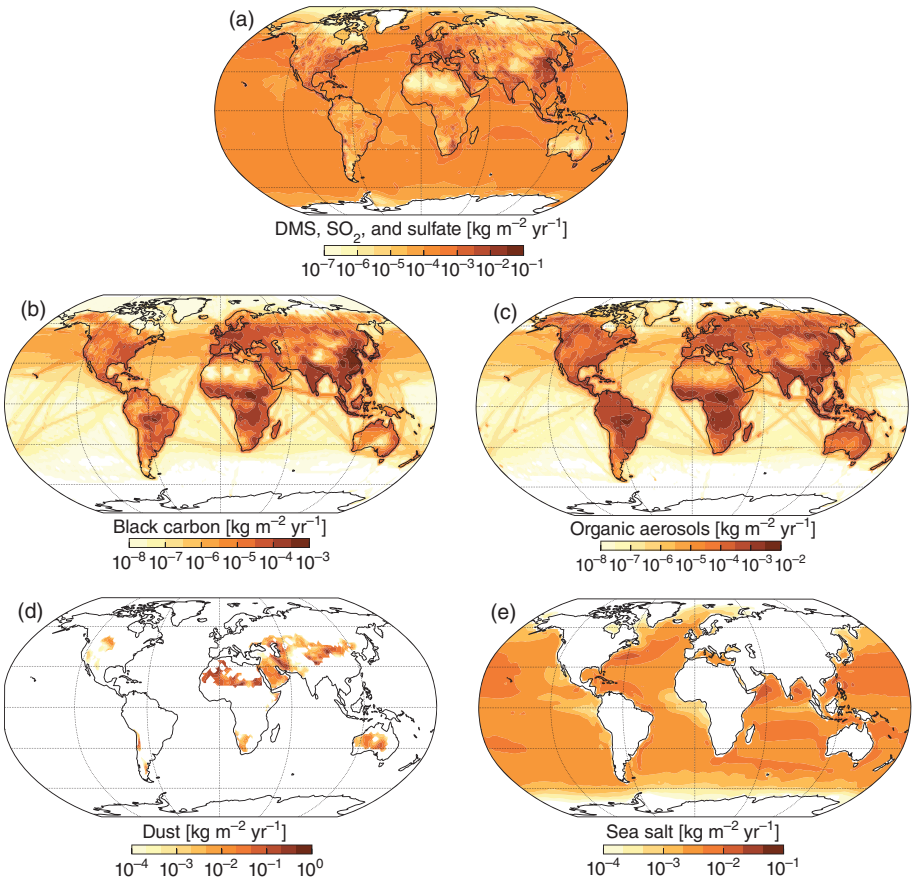


Figure 6.7 Annual mean emissions of (a) the sum of Dimethyl sulfide (DMS), SO_2, and primary sulfate particles, (b) BC particles, (c) OA (sum of POA and SOA), (d) mineral dust particles, and (e) sea salt particles, obtained from the ECHAM6-HAM GCM, averaged over the decade 2003–2012 (Tegen et al., 2019; Neubauer et al., 2019). Note that the scale is different for each aerosol type.

BC emissions amount to 8.2 Tg yr^{-1} for the year 2010 (van Marle et al., 2017; Hoesly et al., 2018).

Precursor emissions for nitrate aerosols occur in the form of NO_x and NH_3 (Fowler et al., 2013). NO_x emissions are dominated by anthropogenic sources. Natural sources include emissions from soils due to microbial production and NO_x from lightning, which produces NO_x directly in the upper troposphere (Schumann and Huntrieser, 2007). For the year 2010, NO_x from soils amounted to 4.7–16.8 Tg N yr^{-1} (Young et al., 2018), and NO_x from lightning to 5.1 $\pm$ 2.0 Tg N yr^{-1} (Griffiths et al., 2021). The anthropogenic sources, including fossil fuel combustion, biomass burning, and other sectors, caused emissions of 44.8 Tg N yr^{-1} (van Marle et al., 2017; Hoesly et al., 2018).

https://doi.org/10.1017/9781009485654.007 Published online by Cambridge University Press

6.4 Aerosol Sinks

Understanding the removal of aerosol particles from the atmosphere is important in order to correctly estimate their atmospheric burdens, lifetimes, and (number) concentrations, which is a key concern for both air quality and climate studies (e.g., von Schneidemesser et al., 2015). This removal is called deposition or scavenging. Broadly, we can distinguish between two categories of scavenging: dry scavenging and wet scavenging. Further subclassification of the scavenging mechanisms depends on the physical processes that are responsible for the removal of the aerosol particles.

Dry scavenging refers to the removal of aerosol particles from the atmosphere by sedimentation due to gravity and the subsequent impaction on Earth's surface. In contrast, the removal of aerosol particles by wet scavenging involves the presence of hydrometeors via two processes: (i) aerosol particles can be removed upon collision with cloud droplets, raindrops, and snowflakes, both in and below clouds, referred to as impaction scavenging; (ii) aerosol particles can become incorporated into hydrometeors, by acting as CCN (Chapter 7) or INPs (Chapter 9). The importance of dry versus wet scavenging has been estimated from coupled global aerosol-climate models. In a study with 12 different GCMs, dry scavenging was found to be the dominant sink for the coarse-mode natural aerosol particles, including sea salt and mineral dust, in the global annual mean. It removes 70–80 % of the aerosol mass in the coarse mode (Textor et al., 2007). For aerosol types that are usually characterized by smaller particles such as sulfate, BC, and OA, wet scavenging is the most important sink, removing 80–90 % of the aerosol mass in the fine mode (Textor et al., 2007).

6.4.1 Wet Scavenging

Wet scavenging (also referred to as wet deposition) is subdivided into impaction scavenging, occurring in- and below-cloud, and nucleation scavenging, occurring only in-cloud.

Impaction Scavenging

Impaction scavenging is a process involving collisions. Here we discuss the collision processes for aerosol particles colliding with any kind of hydrometeor, including cloud droplets, raindrops, ice crystals, snowflakes, graupel, and hailstones. We will discuss collisions of different hydrometeors with each other later in the context of cloud droplet growth (Section 8.2) and ice crystal growth (Section 9.3.3).

Impaction scavenging is described in terms of the *collection efficiency* $\tilde{E}$ between a collecting hydrometeor (also referred to as the collector drop) and the collected aerosol particle. It is the product of the *collision efficiency* E times the *coagulation efficiency* $\hat{E}$, where coagulation means that the two colliding particles remain together after collision.

A schematic of the collision process is shown in Figure 6.8a: a collecting hydrometeor with radius R falls down and sweeps out a volume of air $V_{sweep} = hA_{geo} = \pi(R + r)^2$, which is the

https://doi.org/10.1017/9781009485654.007 Published online by Cambridge University Press

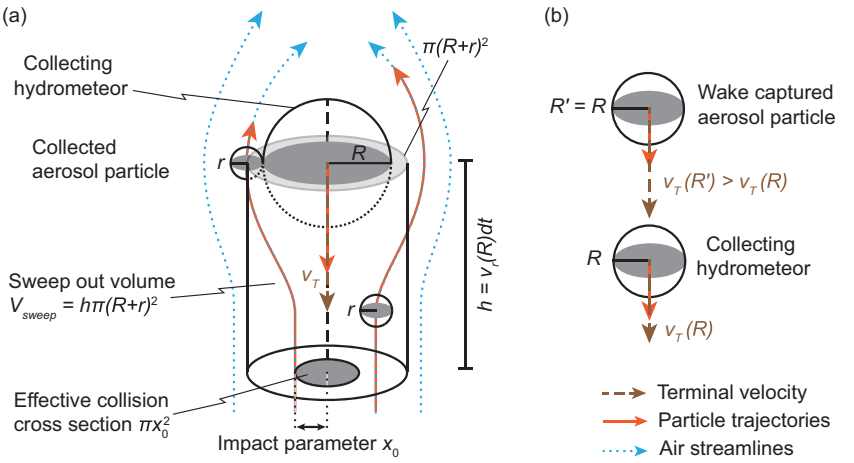


Figure 6.8 (a) Schematic outlining the collision process of a collector drop with radius R and two smaller particles with radius r. The sweep-out volume is given by $V_{sweep} = hA_{geo} = h\pi(R+r)^2$. Further, x_0 denotes the impact parameter and πx_0^2 defines the effective collision cross section. (b) Illustration of the wake capture effect, where the trailing particle collides with the collector drop, because the upper particle is in the wind shadow of it.

product of the distance fallen h times the geometric cross-sectional area A_{geo} of a disk whose radius is the sum of the radii of the falling hydrometeor with radius R and the collected particle of radius r. Here, $h = v_r dt$ is the distance through which the collector drop falls during a time interval dt and v_r is the difference in terminal velocity between the collecting hydrometeor of radius R and the collected aerosol particle of radius r.

In the absence of interactions of the surrounding air with the hydrometeor and the aerosol particles, the collecting hydrometeor would collide with all smaller particles in its path. However, in a medium such as air, the falling collector drop displaces the surrounding air. Since small particles tend to follow the streamlines of the air flow, the (effective) collision process depends on two things, (i) the inertia of the small particles and (ii) the Reynolds number (eq. 8.39) of the collector drop. Only particles with enough inertia, such as the left particle in Figure 6.9a, cross the streamlines of the surrounding air flow and thus collide with the collector drop if they are close enough to its center. Particles further away from the center of the collector drop, such as the right particle in Figure 6.8a, follow the movement of the air around the collector drop and do not collide with it. Large Reynolds numbers Re cause turbulence (random and irregular fluctuations in the air) around the collector drop, which increases the probability of aerosol particles colliding with it.

On the whole, these effects lead to the net result that not every particle within V_{sweep} of a falling hydrometeor collides with it. This fact is taken into account by the collision efficiency E, which provides the fraction of particles with radius r that collide with the falling collector drop with radius R compared with the total number of particles in the sweep-out volume:

https://doi.org/10.1017/9781009485654.007 Published online by Cambridge University Press

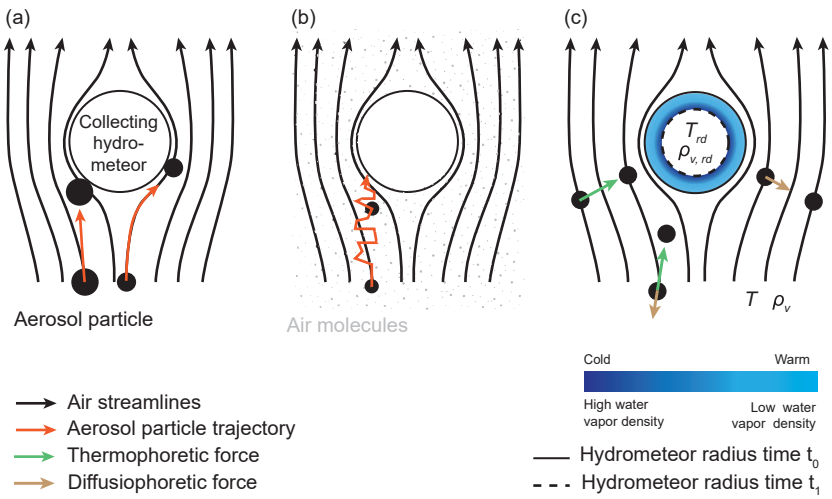


Figure 6.9 Schematic of the different forces and processes that can contribute to a collision between an aerosol particle and a hydrometeor: (a) inertial impaction (left) and interception (right), (b) Brownian motion, and (c) thermophoresis (left), diffusiophoresis (right), and combined phoresis (below) for an evaporating drop. The outlines of the evaporating hydrometeor for different times are indicated by the solid and dashed contours, respectively. The colored arrows show the direction of the forces for an evaporating drop. As different processes are size-dependent, aerosol particles are shown in different sizes. T is the environmental air temperature, T_{r_d} is the temperature at the hydrometeor's surface, ρ_v is the environmental water vapor density, and ρ_{v,r_d} is the water vapor density at the hydrometeor's surface.

$$E(R, r) = \frac{\pi x_0^2}{\pi (R + r)^2}. \tag{6.19}$$

Here, $A_{eff} = \pi x_0^2$ defines the effective collision cross section, where x_0 is the impact parameter within which a collision is likely to occur, whereas outside x_0, particles are likely to be deflected out of the path of the collector drop (see right particle in Figure 6.8a). Due to the random positions of the particles, E can also be interpreted as the probability that the collector drop will collide with a smaller particle located at random in the sweep-out volume. In the presence of turbulence, particles within x_0 could be moved out of it. Likewise, particles outside x_0 may nevertheless collide with the collector drop. While these effects can cancel each other for weak turbulence, the net effect of strong turbulence is an enhancement in collisions, as found from numerical studies of cloud droplet collisions (Wang and Grabowski, 2009; Grabowski and Wang, 2013; Franklin, 2014, Section 8.2.5).

The processes that can cause collisions of an aerosol particle with a falling raindrop or snowflake are shown in Figure 6.9. Collisions can be caused by inertial impaction (Figure 6.9a, left particle) and by interception of the collector drop (Figure 6.9a, right particle). Scavenging

https://doi.org/10.1017/9781009485654.007 Published online by Cambridge University Press

by interception occurs when the particle is small enough to follow the streamlines around the collector drop but gets so close to the collector drop that it is "intercepted".

Other processes that can cause collisions between aerosol particles and a hydrometeor are Brownian[1] motion (Figure 6.9b) or phoretic forces, those which cause the motion of aerosol particles via a temperature, water vapor, or electrical gradient (Figure 6.9c).

Brownian motion refers to microscopic diffusion on a single-particle level. It results from the continuous bombardment of an aerosol particle by the molecules of the surrounding medium: each time the particle is hit by a gas molecule, momentum is transferred to it, causing it to change its direction of movement. This leads to a "random walk" of the particles, called Brownian motion.

Scavenging due to phoretic forces, which act at spatial scale of a millimeter or less, includes thermophoresis and diffusiophoresis (Bae et al., 2009; Santachiara et al., 2013; Cherrier et al., 2017), and electrophoresis (Wang and Pruppacher, 1977; Dépée et al., 2019; Tinsley et al., 2000). The role of electrophoresis depends strongly on the amount of charges present on both the droplet and the aerosol particles (Wang et al., 1978; Nagare et al., 2015). For simplicity, we limit our discussion to thermo- and diffusiophoresis (Figure 6.9c).

The underlying mechanism of thermophoretic processes is reflected in the word *thermophoresis*, from the Greek "carried by heat". A temperature gradient leads to a gradient in the thermal energy of the air molecules, which means that the average velocity of air molecules colliding with an aerosol particle is higher on its warmer side than on its colder side. This, in turn, leads to net movement of the aerosol particle toward the cooler side. A temperature gradient can also be established due to the latent heat. For example, let us consider the case of latent heat consumption of an evaporating hydrometeor: the thermophoretic force will push the aerosol particle along the negative temperature gradient, toward the cool spot of the evaporating hydrometeor. This can be understood as a thermophoretic attraction, leading to wet scavenging if the hydrometeor reaches the ground. By contrast, condensation of water vapor onto a hydrometeor releases latent heat, leading to thermophoretic repulsion of the aerosol particles away from the hydrometeor.

When a hydrometeor evaporates, the increase in water vapor due to the evaporation leads to a net drift of water vapor molecules away from the hydrometeor. This drift is (partly) transferred to the aerosol particles in the vicinity of the hydrometeor, causing them to move in the direction of the diffusive water vapor flux, which is thus called *diffusiophoresis*. For a growing hydrometeor, on the other hand, diffusiophoresis causes a net drift of water molecules toward the hydrometeor that also moves aerosol particles toward the hydrometeor. Here, diffusiophoresis acts as a sink for aerosols. Facy (1955) was among the first to observe the phenomena of thermo- and diffusiophoresis, by noting that evaporating droplets develop a particle-free space in their vicinity.

The water vapor and temperature gradient are always of opposite sign for evaporating or growing hydrometeors. Specifically, thermophoresis is directed toward an evaporating

[1] www.britannica.com/biography/Robert-Brown-Scottish-botanist

https://doi.org/10.1017/9781009485654.007 Published online by Cambridge University Press

hydrometeor and diffusiophoresis away from it, and vice versa for a growing hydrometeor. Overall, thermophoresis is the dominant force (see the arrows in Figure 6.9c for their magnitudes and Figure 6.10).

On the whole, the impaction scavenging process by which aerosol particles are removed from the atmosphere depends strongly on the size of the aerosol particles, as shown in Figure 6.10. As can be seen, the collection efficiency for wet deposition has a minimum for accumulation-mode particles. This minimum in wet deposition coincides with the minimum in dry deposition and is commonly referred to as the *Greenfield gap* (Greenfield, 1957).

For small particles, Brownian motion is the dominant wet scavenging process and can cause the collision of these particles with a falling hydrometeor (Figure 6.10). For aerosol particles with radii $> 0.5\,\mu m$, inertial impaction and interception are the most important forces since particles in this size range do not follow the streamlines of the air around a falling hydrometeor but instead deviate from them toward the hydrometeor and may collide with it.

Phoretic forces contribute to the overall collection efficiency mainly for aerosol particles of intermediate sizes, mostly those in the accumulation mode, where both Brownian motion and inertial forces are small (Santachiara et al., 2013). The exact size ranges corresponding to the importance of the different forces for aerosol scavenging depend on the size of the falling hydrometeor and, if applicable, on the evaporation or sublimation rate of the hydrometeor. The higher its evaporation or sublimation rate, the larger is the contribution from thermophoresis. For aerosol particles less than 10 nm, particle motion due to Brownian motion is sufficiently random that thermo- and diffusiophoresis do not induce an unidirectional movement (Figure 6.10).

The process of collection requires not only a collision but also the subsequent coagulation of the collision partners, such that they do not separate again after the collision. The coagulation efficiency $\hat{E}$ of an aerosol particle with a liquid particle (cloud droplet or raindrop) is assumed to be unity, so that every particle coming into contact with a liquid particle becomes incorporated into it (Croft et al., 2009). Therefore, $\tilde{E} = E$ and thus the size dependence of $\tilde{E}$ shown in Figure 6.10 reflects the size dependence of E.

Figure 6.11 shows the collection efficiency $\tilde{E}$ for collisions of a liquid drop of varying size with aerosol particles between 1 nm and 50 μm in radius. It can be seen that for giant aerosol particles larger than 5 μm in radius, collision with an approaching drop is virtually inevitable, whereas only one in 10^3 to 10^5 accumulation mode particles with radii between 0.05 and 0.5μm in the sweep-out volume of a falling drop ends up colliding with it. Certainly, at a given aerosol size, there is also a dependence of the collection efficiency on the size of the liquid collector drop: The larger the liquid collector drop, the higher the collection efficiency for supermicron aerosol particles. The reverse is true for submicron aerosol particles. In addition, the below-cloud wet scavenging of aerosol particles has been observed to depend on other parameters, such as rain rate (Laakso et al., 2003).

Yet another mechanism by which accumulation mode aerosol particles are effectively removed from the atmosphere is through *wake-capture* (e.g., Lemaitre et al., 2017). During wake- or rear-capture, the aerosol particle is drawn into the rear of the falling collector droplet

https://doi.org/10.1017/9781009485654.007 Published online by Cambridge University Press

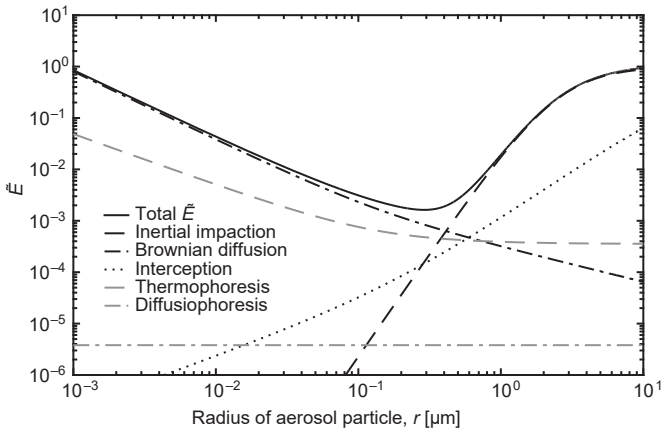


Figure 6.10 Theoretical calculations of different forces contributing to the total collection efficiency $\tilde{E}$ for hydrometeor-aerosol collisions as a function of aerosol particle radius r. In the calculations, the evaporating liquid hydrometeor had an initial radius of 40 μm at $T = 245$ K and was kept at ice saturation. The parameterizations are taken from Park, Jung, Jung, Lee and Lee (2005) for Brownian diffusion, inertial impaction, and interception, and from Andronache et al. (2006) for thermophoresis and diffusiophoresis. Figure adapted from Nagare et al. (2015).

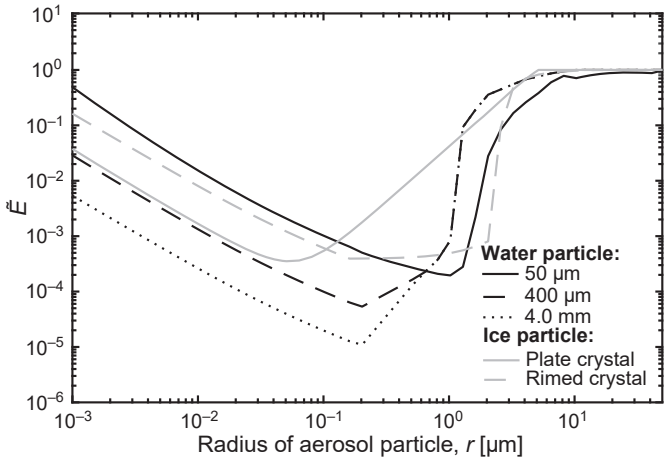


Figure 6.11 Below-cloud collection efficiency $\tilde{E}$ for raindrop-aerosol collisions as a function of aerosol radius r and collector raindrop size. In addition, $\tilde{E}$ is shown for below-cloud snowflake-aerosol collections: a plate with an equivalent radius of 500 μm and a rimed crystal with a characteristic dimension of 100 μm. Figure adapted from Croft et al. (2009).

https://doi.org/10.1017/9781009485654.007 Published online by Cambridge University Press

by the re-circulating flow. Because it is in the wind shadow of the collector droplet and hence experiences less drag, it ultimately collides with the collector drop at its rear side (Fig. 6.8b).

Figure 6.11 also shows the collection efficiency for collisions of two different snowflake types with aerosol particles. The removal of aerosol particles by falling snowflakes was found to be similar and of the same order of magnitude as that for removal by smaller raindrops in the study by Croft et al. (2009). The removal of aerosol particles by snowflakes further depends on the morphology of the snowflake. In Figure 6.11, two estimates of the aerosol collection efficiency of snowflakes of two different shapes are shown: for a plate with an equivalent radius of 500 μm and for a rimed crystal with a characteristic dimension of 100 μm (Croft et al., 2009). As in the case of the rain drop, the smaller the snowflake, the higher the collection efficiency of nucleation and Aitken mode particles. The reason is that larger hydrometeors disturb the streamlines of the approaching particles more and therefore a larger fraction of the fine-mode particles has a chance to become reflected around the collector hydrometeor. For coarse-mode particles, this effect becomes negligible or is even reversed because of their large inertia, which drives them toward the collector hydrometeor. In general, the removal of aerosol particles by snowflakes is more uncertain than their removal by rain drops. In contrast to the findings shown in Figure 6.11, other studies have reported impaction scavenging in liquid-phase clouds to be considerably greater than in ice-phase clouds. For example, Browse et al. (2012) have reported that the seasonal variation of BC and sulfate aerosol number concentrations in the Arctic is such that there are high concentrations in wintertime and low concentrations in summer time, caused by a transition from ice-phase cloud to liquid-phase cloud scavenging. Similarly scavenging of BC in Arctic clouds was found to be positively correlated with cloud liquid water content (Zieger et al., 2023).

Nucleation Scavenging

Given that accumulation mode aerosol particles are poorly removed by either dry or collision-induced wet scavenging, there must be another way in which they are removed from the atmosphere. In fact, accumulation mode particles are most efficiently removed by *nucleation scavenging* (Wurzler et al., 1995; Croft et al., 2010). Nucleation scavenging refers to the ability of aerosols to act as CCN or INPs and to be incorporated into a hydrometeor that grows to precipitation size and finally reaches the ground as precipitation. The ability of aerosol particles to act as CCN or INPs depends, along with other physico-chemical characteristics, strongly on size, as will be discussed in Chapters 7 and 9.

An example of how nucleation scavenging removes first the largest particles and subsequently smaller and smaller particles is shown in Figure 6.12. The trend mimics the way in which aerosol particles act as CCN in that the largest particles are activated first (Section 7.5.2). The degree of supersaturation in the cloud determines the size above which aerosol particles can be activated. The higher the supersaturation, the smaller the aerosol particles that can activate and thus be subject to nucleation scavenging. If the supersaturation is sufficiently high, some Aitken mode particles can even act as CCN and hence be subject to nucleation scavenging. If all aerosol particles have the same chemical composition, all particles with sizes equal or larger to a critical radius, termed r_{crit}, will undergo nucleation scavenging

https://doi.org/10.1017/9781009485654.007 Published online by Cambridge University Press

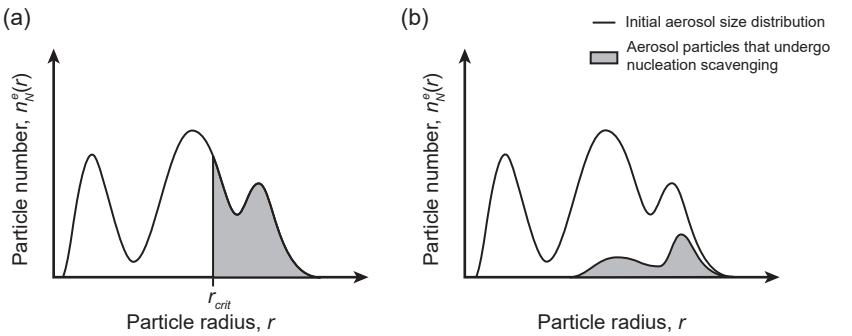


Figure 6.12 Schematic of an aerosol number size distribution illustrating the effect of nucleation scavenging, where the gray shaded area denotes the aerosol particles that undergo nucleation scavenging. Different aerosol populations are shown: (a) aerosol particles with uniform chemical composition and (b) an aerosol population with both internally and externally mixed particles and a size-dependent chemical composition.

(Figure 6.12a). Specifically, for a given supersaturation, these aerosol particles will activate and form cloud droplets (Chapter 7).

By contrast, for an aerosol population where the chemical composition varies as a function of particle size, not all of the largest aerosol particles will undergo nucleation scavenging and act as CCN (Figure 6.12b). This is due to the difference in their composition and the differing ability of different materials to take up water and form cloud droplets, as we will see in Chapter 7.

A similar logic applies to nucleation scavenging in ice clouds, where aerosol particles can act as INPs. As the number of aerosols acting as INPs compared to CCN is much fewer, nucleation scavenging is only of minor importance in ice clouds (e.g., Stier et al., 2005; Croft et al., 2010).

6.4.2 Dry Scavenging

Dry scavenging occurs when particles that are still suspended in the atmosphere, but very close to the surface, are deposited onto a surface (Farmer et al., 2021). It has been found useful to describe dry deposition in terms of a *dry deposition velocity* (Figure 6.13). This is an effective velocity, which describes how quickly an aerosol particle makes contact with the surface. It depends on the aerosol's size, density, and morphology as well as to the properties of Earth' surface such as the surface roughness and the amount of turbulence present. As an example, dry deposition velocities are generally higher over forests, which have a larger surface roughness compared to grassland surfaces (Figure 6.13). The dry deposition velocity is smallest for accumulation-size aerosol particles and increases toward smaller sizes due to Brownian motion.

Brownian motion speeds up the dry deposition of the smallest particles. This is because the random walk for such small particles has an amplitude that is large enough that particles in the vicinity of Earth's surface collide with it and are thus removed at a considerable

https://doi.org/10.1017/9781009485654.007 Published online by Cambridge University Press

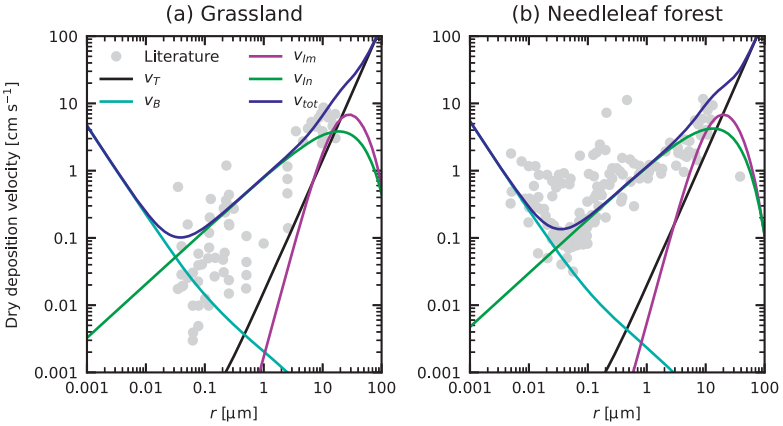


Figure 6.13 Dry deposition velocity of aerosol particles over different surfaces, (a) grassland and (b) needleleaf forest, as a function of their radius. Also shown is a parameterization of the dry deposition velocity v_{tot} at 293.15 K and 1013.25 hPa and its individual contributions: terminal velocity due to gravity v_T for aerosol particles of 1200 kg m^{-3} over grassland and aerosol particles of 1500 kg m^{-3} over needleleaf forest according to Emerson et al. (2020), and velocity due to Brownian diffusion v_B, impaction v_{Im}, and interception v_{In}, using the Stokes number for vegetated surfaces according to Zhang et al. (2001). Figure reproduced from Emerson et al. (2020).

rate. This leads to a larger net-averaged downward velocity (i.e., dry deposition velocity) than that for accumulation mode particles. Particle diffusion, on the other hand, is much slower than the diffusion of the gas molecules, making its diffusion coefficient orders of magnitude smaller.

The dry deposition velocity for small aerosol particles is thus dominated by Brownian motion. For these small aerosol particles the dry deposition velocity is proportional to the Schmidt[2] number Sc to the power $-2/3$, as indicated in Figure 6.13. The Sc number is the ratio of the viscous diffusion rate and the molecular diffusion rate. Sc can be described in terms of the kinematic viscosity in air ν and the mass diffusivity D_a (also referred to as diffusion rate) of the aerosol particle in the air:

$$Sc = \frac{\nu}{D_a} = \frac{\mu}{\rho_a D_a}. \tag{6.20}$$

Note that D_a depends inversely on the aerosol radius. Instead of the kinematic viscosity, the dynamic viscosity μ can be used. μ and ν are related by the density of air ($\mu = \rho_a \nu$).

The dry deposition velocity increases for particles with a radius larger than ~0.05 µm, when interception scavenging (Figure 6.9) becomes the dominant force. For particles larger than ~10 µm, impaction scavenging and gravitational settling start to become the dominant forces (Figure 6.13). Gravitational setting will be revisited in Section 8.2.2 for hydrometeors. Dry deposition is the dominant sink for coarse-mode aerosol particles. For smaller particles, the dry deposition velocity is so small that the particles rather undergo one of the processes leading to wet deposition.

[2] https://de.wikipedia.org/wiki/Ernst_Schmidt_(Thermodynamiker)

https://doi.org/10.1017/9781009485654.007 Published online by Cambridge University Press

6.4.3 Atmospheric Processing of Aerosol Particles

Prior to being removed from the atmosphere, aerosol particles can undergo various aging processes when travelling through the atmosphere. Aging of aerosol particles generally refers to any alteration of the particle's chemical or physical properties. Atmospheric aging processes include heterogeneous processes, such as adsorption of (trace) gas species or oxidation of the particles by gaseous oxidants such as ozone (e.g., Ammann et al., 1998; Song and Carmichael, 1999; Rudich et al., 2007); condensation of vapors leading to coatings or coagulation with other aerosol types (e.g., Schwarz et al., 2008; Fierce et al., 2015); multiphase reactions, such as oligomerization in the particle phase or condensed phase oxidation (e.g., Kalberer et al., 2004; Herrmann et al., 2015); photochemical processing induced by solar radiation (e.g., George et al., 2015; Al-Abadleh, 2021); and cloud processing (e.g., Pruppacher and Jaenicke, 1995; Mahrt et al., 2020).

An example of a chemical aging process is the reactive uptake of ammonia gas (NH_3) by sulfuric acid (H_2SO_4) particles (e.g., Huntzicker et al., 1980). This results in either ammonium bisulfate (NH_4HSO_4) or ammonium sulfate ($(NH_4)_2SO_4$), depending on the amount of ammonia gas available:

$$H_2SO_4(aq) + NH_3(g) \rightarrow NH_4HSO_4(aq), \tag{6.21}$$

$$H_2SO_4(aq) + 2NH_3(g) \rightarrow (NH_4)_2SO_4(aq). \tag{6.22}$$

An example of a physical aging process is changes in particle shape. For instance, freshly emitted BC particles are often open, fractal-like structures, which can become restructured into more compact aggregate shapes upon aging (e.g., Corbin et al., 2023), by, for example, condensation or evaporation of semi-volatile organic compounds and water (e.g., China et al., 2015).

A change in the physical and/or chemical properties of the aerosol particles can change their impact on atmospheric processes. In fact, aging can alter their chemical reactivity (e.g., Folkers et al., 2003), optical properties, ability to interact with water, and thus abilities to act as CCN (e.g., Friebel et al., 2019) and INPs (e.g., Mahrt et al., 2020).

As an example of aging-induced changes in reactivity, consider the heterogeneous uptake of N_2O_5 (Dentener and Crutzen, 1993). The reactive uptake of N_2O_5 on aerosol particles, leading to a reduction of the gas phase pollutants NO_2 and O_3 is efficient on aqueous aerosol particles, but can be considerably reduced in the presence of an organic coating around the particle that can form as a result of aging (e.g., Folkers et al., 2003; Cosman et al., 2008).

Aging can also change the ability of an aerosol particle to take up water vapor, which depends on its chemical composition and mixing state. In general, a particle may be described as hygroscopic, hydrophilic, or hydrophobic.

Hydrophilic particles are solid particles that can be wetted by water and may dissolve in water. *Hygroscopic* aerosols are hydrophilic particles that readily take up water vapor from the atmosphere and retain it. Water uptake can take place by adsorption at the surface of the particle or absorption when the water molecules penetrate the surface and enter the bulk of the aerosol particle. Examples of hygroscopic particles are salts such as ammonium sulfate ($(NH_4)_2SO_4$), sodium nitrate ($NaNO_3$), and sodium chloride (NaCl). *Hydrophobic* aerosol

https://doi.org/10.1017/9781009485654.007 Published online by Cambridge University Press

particles, such as freshly emitted BC, are the opposite of hydrophilic particles and as such do not like to be wetted by water. Hydrophobic aerosol particles can be removed only by dry deposition or wet impaction scavenging, but not by nucleation scavenging.

Atmospheric aging of fresh BC particles can change their interaction with water vapor and over time render the particles hydrophilic (Zuberi et al., 2005) or even hygroscopic, if sufficient amounts of sulfuric acid or another hygroscopic substance condense on it (Zhang et al., 2008). For instance, aging of BC particles by exposure to ozone has been shown to alter the surface oxidation (Friebel and Mensah, 2019), which makes the BC particles more hydrophilic (Chughtai et al., 1999; Wei et al., 2017), ultimately enhancing water adsorption and their ability to act as CCN (Friebel et al., 2019). Similarly, if BC acquire water-soluble material either by the collisions with other particles that contain soluble material or by condensation of sulfuric acid or organics from the vapor phase, its mixing state changes from externally mixed to internally mixed (Riemer et al., 2009). The changes in the particle mixing state can cause the BC particles to become hygroscopic (Khalizov et al., 2009; Pagels et al., 2009), ultimately enhancing their ability to serve as CCN and INPs in clouds (Zhang et al., 2008; Gao et al., 2022).

Aging processes can also impact the particle size distribution. For example, coagulation or condensation of semi-volatile species can transfer nucleation mode particles to Aitken mode particles and Aitken mode particles further into accumulation mode particles (e.g., Capes et al., 2008; Stolzenburg et al., 2018; Mohr et al., 2019).

Another example is the aqueous-phase oxidation of SO_2 with H_2O_2 or O_3 in cloud droplets to form SO_4 (Lohmann et al., 1999). If the cloud droplet subsequently evaporates, it leaves a larger aerosol mass behind compared to the aerosol mass it formed on. As the size distribution of the non-activated aerosol particles remains the same, a bimodal distribution often appears between those aerosols that acted as CCN and the non-activated aerosol particles, leading to a bimodal aerosol distribution (Hudson and Noble, 2021). This gap has been termed the *Hoppel minimum* (Hoppel et al., 1994).

6.5 Burden and Lifetime of Aerosols

The vertically integrated amount of aerosol particles that resides in the atmosphere is the *aerosol burden*. The aerosol burden can be obtained from simulations with global Earth system models considering various aerosol sources (Section 6.3) and aerosol sinks (Section 6.4), and is typically presented as a multi-annual mean. The *lifetime* of an aerosol type is then estimated as the ratio of the burden and the emissions of a given aerosol type. Table 6.4 lists estimates of the aerosol burden and lifetimes, obtained from an aerosol model intercomparison involving 14 global aerosol climate models (Gliß et al., 2021). An example of the geographical distribution of the various aerosol burdens, obtained from one of these models, ECHAM6-HAM GCM (Tegen et al., 2019), averaged over the decade 2003–2012, is shown in Figure 6.14.

From Figure 6.14 and Table 6.4, it becomes evident that mineral dust dominates the aerosol burden, even though the mineral dust emissions are only 30 % of those of sea salt. This is caused by the different mechanisms by which these aerosol types are injected into and removed from

https://doi.org/10.1017/9781009485654.007 Published online by Cambridge University Press

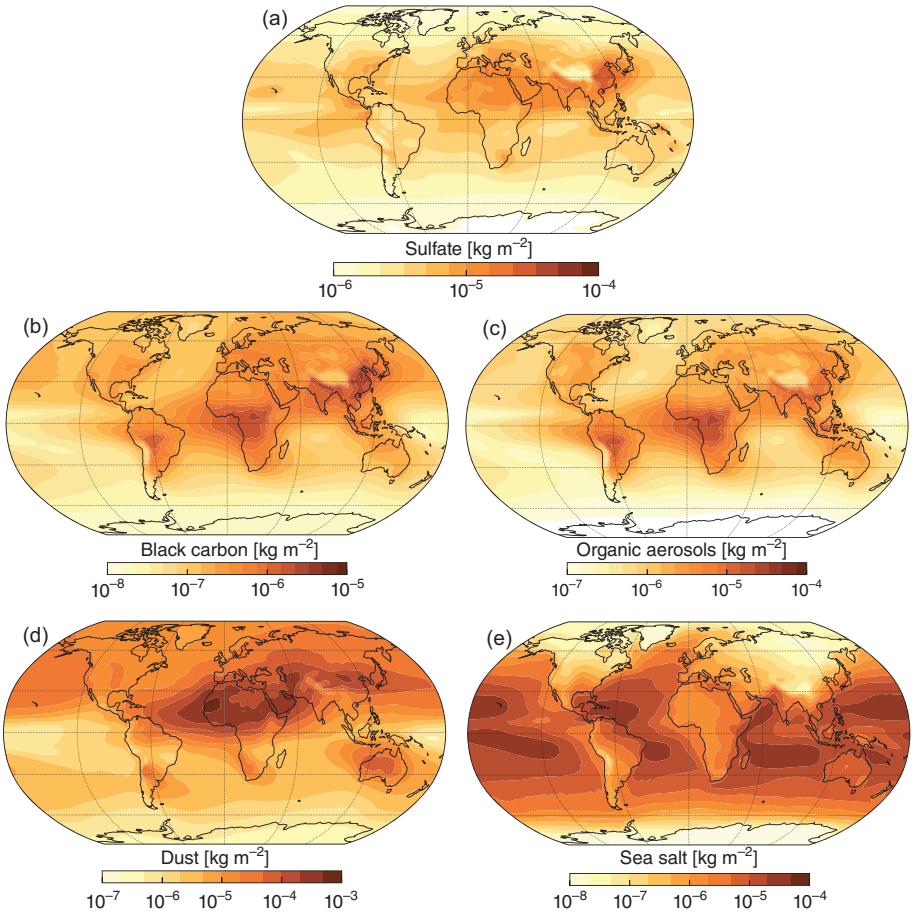


Figure 6.14 Annual mean aerosol burden averaged over the decade 2003–2012 of (a) sulfate, (b) BC, (c) OA (sum of POA and SOA), (d) mineral dust, and (e) sea salt particles, from a global simulation with the ECHAM6-HAM GCM (Tegen et al., 2019; Neubauer et al., 2019). Note that the scale is different for each aerosol component.

the atmosphere, which together determine the lifetimes of these aerosol types. Dust storms and deep dry convection can transport the mineral dust aerosols rather high into the atmosphere (Prospero and Carlson, 1972; Tsamalis et al., 2013; Xu et al., 2018). For instance, particles from the Taklamakan or the Sahara desert are often entrained to altitudes > 5 km and thus enter the free troposphere. Sometimes mineral dust is lifted up in deep convective clouds and reaches even higher altitudes. Upon reaching high altitudes, the mineral dust can undergo long-range transport, for example, from their source regions all the way to North and South America (Engelstaedter et al., 2006; van der Does et al., 2018; Nogueira et al., 2021). As the lifetime of aerosol particles increases with altitude (Figure 6.15a), the higher the mineral dust particles are injected into the atmosphere, the longer their lifetime and thus the higher their burden. In contrast, sea salt has the largest emission rate (Table 6.4). However, these particles remain near the surface in humid air, where they are removed efficiently by wet and dry deposition. As the sea salt emissions are strongly wind-speed dependent (Fairall et al., 1983;

https://doi.org/10.1017/9781009485654.007 Published online by Cambridge University Press

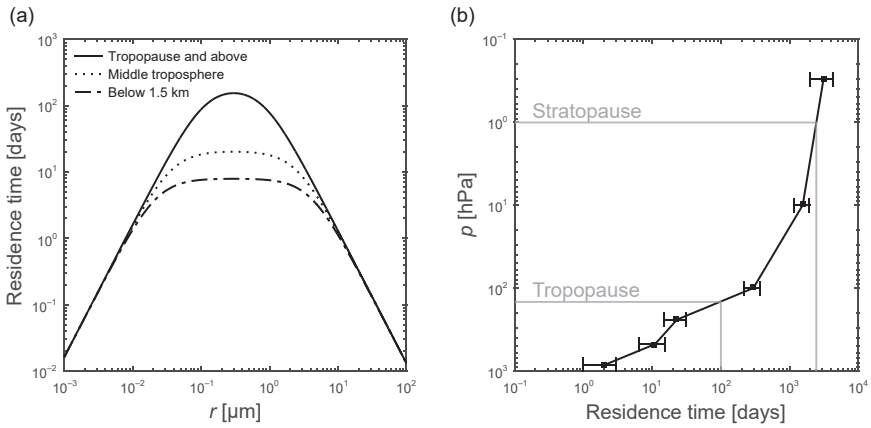


Figure 6.15 Lifetime of aerosols (a) as a function of size for different levels in the atmosphere and (b) as a function of pressure. Figure adapted from Jaenicke (1988) (a) and from Flohn (1973) (b) with permission from Springer Science and Business Media.

Andreas, 1998), high sea salt emission rates are often produced by storms, which also remove these particles very efficiently. Thus, the lifetime of sea salt particles (half a day) is the shortest of the different aerosol species included in Table 6.4. This explains its rather small burden compared to that of mineral dust. Consequently, atmospheric transport of sea salt is also limited, which further elucidates why little sea salt is found over the continents (Figure 6.14e). In summary, because of the much shorter lifetimes of aerosol particles as compared to well-mixed greenhouse gases (WMGHGs), the aerosol burdens are highly variable spatially.

Of the four aerosol species dominated by anthropogenic emissions (nitrate particles, sulfate particles, BC particles, and POA), nitrate particles have the shortest lifetime of just 3 days. The lifetimes of BC particles and POA are on average 1.5–2 days longer than those of nitrate particles (Table 6.4). This is because these particles are generally more hydrophobic upon emission and first need to become internally mixed with more hygroscopic aerosol species, before they can be removed by nucleation scavenging. In addition, BC aggregates usually have a low density, resulting in a slow gravitational settling. The sulfate aerosol burden is highest in the northern hemisphere in proximity to the major industrial sources in Southeast Asia, whereas the POA burden is highest in regions with biomass burning in South America and Africa. The BC aerosol burden shows a similar pattern to that of POA, but it has a third maximum in Southeast Asia.

Overall, both dry and wet scavenging efficiencies are smallest for the accumulation mode, causing their lifetimes to be longest (Figure 6.15a). On the one hand, the lifetime decreases for smaller particles because of Brownian motion, which can result in a collision with either a hydrometeor (Figure 6.10) or with another aerosol particle, forming a larger particle. On the other hand, the lifetime decreases for larger particles because of gravitational settling (Figure 6.13), and an increased probability of nucleation scavenging by acting as CCN and INPs.

However, the lifetime not only depends on particle size, but also on the altitude where the particle is located (Figure 6.15b). For example, the average lifetimes of accumulation mode

https://doi.org/10.1017/9781009485654.007 Published online by Cambridge University Press

particles are around one week in the lowest 1.5 km of the troposphere, two weeks in the mid-troposphere, around 100 days in the tropopause region, and typically reach several years in the stratosphere.

One of the most abundant aerosols in the stratosphere are sulfate particles. They result from major volcanic eruptions, such as the Mount Pinatubo eruption in June 1991, which injected large amounts of gaseous sulfur dioxide (SO_2) into the upper troposphere and stratosphere (McCormick et al., 1995). The SO_2 is subsequently oxidized to gaseous sulfuric acid and further nucleates to either form sulfate aerosols (Section 6.3.1) or to condense onto pre-existing aerosol particles (e.g., Wilson et al., 1993). The very long (multi-year) lifetime of stratospheric sulfate aerosols results from the fact that gravitational settling is the only sink. A typical mode radius for stratospheric sulfate aerosols formed by gas-to-particle conversion with subsequent coagulation after a volcanic eruption is 0.3 μm (Timmreck et al., 1999). This radius lies in the Greenfield gap, between removal by collisions due to Brownian motion and removal by inertial impaction. A particle with 0.3 μm radius has a sedimentation velocity on the order of 0.01 mm s^{-1}. Thus, it would take more than 1 year for such a particle to settle 1 km, assuming a spherical particle with a density of that of sulfuric acid (Table 6.2). In reality, however, some coagulation will occur. In addition, the sulfate aerosols will be subject to wet deposition once they enter the troposphere.

The long lifetime of particles in the stratosphere is evident as a layer of a high aerosol number concentration (mainly sulfate aerosols) exists between the tropopause and approximately 30 km altitude. This layer is often referred to as *Stratospheric Aerosol Layer* or *Junge*[3] *layer* (Junge et al., 1961*a*,*b*; Junge and Manson, 1961).

This aerosol layer and the long lifetime of stratospheric particles are one reason behind the idea that part of the global warming caused by anthropogenic activities could be offset by injecting aerosols into the stratosphere (Crutzen, 2006). This is referred to as climate intervention and will be discussed in Section 12.4.

6.6 Summary of Aerosol Processes

A summary of the main aerosol processes as a function of aerosol radius is shown in Figure 6.16. Nucleation mode aerosols originate from gas-to-particle conversion and are commonly found over vegetation such as forests that emit large quantities of VOCs, which are precursors to SOA particles. In addition, sulfuric acid nucleation mode particles frequently form in the upper troposphere (e.g., Lucas and Prinn, 2003). Aitken mode particles are mainly emitted during combustion processes of which the most important sources are related to anthropogenic activities. These aerosol particles form predominantly by gas-to-particle conversion producing secondary particles. Combustion processes also emit large quantities of BC and POA that are considered as primary particles. Other important sources of BC and POA are biomass burning and wildfires, which also emit large amounts of organic vapors that can become oxidized and form SOA.

[3] https://de.wikipedia.org/wiki/Christian_Junge

https://doi.org/10.1017/9781009485654.007 Published online by Cambridge University Press

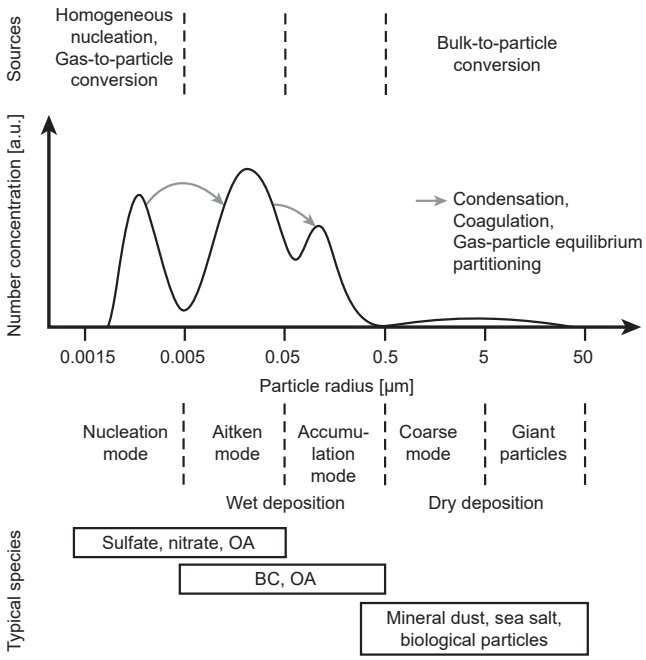


Figure 6.16 Schematic of the main aerosol sources, transformation and removal processes for typical species as a function of their size. BC refers to black carbon and OA to organic aerosol.

All particles can grow by condensation of supersaturated gas species, equilibrium gas-particle partitioning, or, if they are sufficiently hygroscopic, by water vapor uptake. In addition, collection (collision and coagulation) of different aerosol particles shifts them to larger sizes. This internal redistribution is especially important as a sink for nucleation mode particles, transferring them to Aitken mode particles. It is still also important for Aitken mode particles that are transferred to accumulation mode particles but is a negligible growth process of accumulation mode particles, because they have a very small collection kernel. The Collection of aerosol particles is linked to their mobility. Their mobility rapidly decreases as their size increases, confining collection due to Brownian motion to nucleation and Aitken mode particles.

The source of coarse mode particles is bulk-to-particle or liquid-to-particle conversion. Here, dry deposition is the main removal mechanism, which increases in importance with increasing particle size. For comparison, the dry deposition velocity of a spherical aerosol particle with 1 μm radius and unit density is $\sim 0.02\,\mathrm{cm\,s^{-1}}$ and that of a 10 μm aerosol particle is $2\,\mathrm{cm\,s^{-1}}$ (Figure 6.13).

The main sink of accumulation mode particles is by them acting as CCN and being removed by nucleation scavenging if the cloud precipitates. Nucleation scavenging also removes coarse mode particles and, depending on the updraft speed, also the larger Aitken mode particles, as will be discussed in the next chapter. Nucleation scavenging further removes those aerosol particles that act as INPs in precipitating mixed-phase and ice clouds (Chapter 9).

https://doi.org/10.1017/9781009485654.007 Published online by Cambridge University Press